NRL Report 7954

Dynamics of Satellite Disintegration

ROBERT DASENBROCK, BERNARD KAUFMAN,
AND WILLIAM HEARD

Systems Research Branch
Space Systems Division

January 30, 1976

NAVAL RESEARCH LABORATORY
Washington, D.C.

SECURITY CLASSIFICATION OF THIS PAGE *(When Data Entered)*

REPORT DOCUMENTATION PAGE		READ INSTRUCTIONS BEFORE COMPLETING FORM
1. REPORT NUMBER NRL Report 7954	2. GOVT ACCESSION NO.	3. RECIPIENT'S CATALOG NUMBER
4. TITLE *(and Subtitle)* DYNAMICS OF SATELLITE DISINTEGRATION		5. TYPE OF REPORT & PERIOD COVERED Final report on NASA Project L5106A 6. PERFORMING ORG. REPORT NUMBER
7. AUTHOR*(s)* Robert Dasenbrock, Bernard Kaufman, and William Heard		8. CONTRACT OR GRANT NUMBER*(s)*
9. PERFORMING ORGANIZATION NAME AND ADDRESS Naval Research Laboratory Washington, D. C. 20375		10. PROGRAM ELEMENT, PROJECT, TASK AREA & WORK UNIT NUMBERS NRL Problem B01-17 Project L5106A
11. CONTROLLING OFFICE NAME AND ADDRESS National Aeronautics and Space Administration Langley Research Center Hampton, Va. 23365		12. REPORT DATE January 30, 1976 13. NUMBER OF PAGES 43
14. MONITORING AGENCY NAME & ADDRESS*(if different from Controlling Office)*		15. SECURITY CLASS. *(of this report)* Unclassified 15a. DECLASSIFICATION/DOWNGRADING SCHEDULE

16. DISTRIBUTION STATEMENT *(of this Report)*

Approved for public release; distribution unlimited.

17. DISTRIBUTION STATEMENT *(of the abstract entered in Block 20, if different from Report)*

18. SUPPLEMENTARY NOTES

19. KEY WORDS *(Continue on reverse side if necessary and identify by block number)*

Satellites; Spacecraft; Artificial satellites; Fragmentation; Fragment clouds; Debris; Collisions; Probability of collision; Statistical mechanics; Orbits; Liouville's theorem

20. ABSTRACT *(Continue on reverse side if necessary and identify by block number)*

Satellite disintegration is examined in detail. Elements of the orbits of individual fragments, determined by DOD space-surveillance systems, are used to accurately determine the time and place of the fragmentation. Dual time-independent and time-dependent analyses are performed for simulated and real breakups. Methods of statistical mechanics are used to study the evolution of the fragment clouds by treating the fragments as an ensemble of noninteracting particles. A solution of Liouville's equation is obtained which enables the spatial density to be calculated as a function of position, time, and initial velocity distribution. Conversely, a relation is established

Continued

20. Continued

between the observed fragment distribution and the time of fragmentation and initial velocity distribution. The probability of collision between a spacecraft and a fragment cloud is calculated.

CONTENTS

DYNAMICS OF SATELLITE DISINTEGRATION

INTRODUCTION AND OVERVIEW

The importance of space debris and the ability to maintain ephemerides of this debris grows increasingly significant each year. The steady growth in the known orbital population means that the probability of a collision between an important spacecraft and another object will continue to increase to the point of real danger. Because the orbital lifetime can be quite long, this debris population will influence the near-earth environment for many years to come. The amount of known material in orbit about the earth has already grown sufficiently large so that concern about collision between spacecraft and debris is now being actively channeled into realistic investigations.

Space debris is created in many ways. Much of it is associated with the main spacecraft and consists of items such as spent rocket bodies, adapter rings, and ordinary nuts and bolts. Occasionally, for various reasons, spacecraft disintegrate or explode in orbit, and a single such catastrophic event can increase the debris population by the hundreds. For example, over 3000 objects are being tracked by NORAD [1], and over half of this observable population can be attributed to spacecraft breakups. It is interesting to note that 1430 current radar-trackable fragments are the result of only ten orbital breakups [2].

Any investigation into the probability of spacecraft collisions runs immediately into the problem of unknown population density, particularly as concerns a spacecraft disintegration. This unknown density arises because not all potentially hazardous objects are of sufficient size to be tracked by current systems. A further complication is added by the accuracy with which objects in orbit can be tracked. This accuracy is in general insufficient for a satisfactory deterministic solution to the collision-probability problem. Nevertheless significant investigations have been made into this increasingly important area.

One of the early investigations into the motion of an orbital debris cloud was by Ross [3] in 1961. He analyzed the orbital characteristics of a cloud of pellets following their release from a spinning container initially in a circular orbit. A further analysis of simulated spacecraft explosions was carried out in separate investigations by Fuss [4] and Gabbard [1] in 1974. The purpose of the latter investigation was to characterize the orbital fragment distribution in order to aid in cataloging the explosion debris. The possibility of collisions between spacecraft and orbital debris has been the subject of investigations by McCarter [5] in 1972 and later by Brooks [2] et al. in 1974. The latter investigation indicates a collision probability for a 1000-day mission of up to 0.08 for certain classes of earth orbiters. This investigation presumes the existence of a high percentage of untrackable objects in space. These objects include those having cross sections less than the approximate 0.01 square meter required to be seen by ground-based radar [2].

Manuscript submitted November 12, 1975.

The reverse aspect of the problem is also of interest, namely, determining the origin of an observed fragment cloud. Once a new collection of objects appears in orbit, NAVSPASUR [6] routinely backdates the position of each individual object to determine if any or all of the set converge to a common origin. Their procedure is to determine the time that minimizes the size of the largest subcluster which lies within a predetermined radius. The "size" is defined as the sum of the squares of the distances to each fragment of this subset from the center of the cluster.

The primary purpose of the present investigation is to further study the dynamical characteristics of an evolving fragment cloud in order to yield insight into both its future evolution for purposes of collision probabilities and to determine how the dynamics might be used to obtain the precise origin of the cloud. Specifically, satellite breakups are simulated to study the characteristics of their evolving fragment clouds. These characteristics are then used to determine how the time and place of a satellite explosion might be accurately determined once its fragment cloud has been observed. Also the accuracy requirements of the data are investigated to determine how much error may be tolerated in the orbital elements and still yield an accurate breakup point.

There are two methods of attacking this overall problem. The first is the historical numerical method based on knowledge of the orbits of individual fragments, and the second is the application of the methods of statistical mechanics whereby the fragment cloud is treated as an ensemble of noninteracting particles. This latter method associates a continuum of particles with the observed population and thereby implicitly interpolates the previously discussed unobserved fragments. Both of these approaches have been adopted in this study.

By the numerical approach the current investigation determines the origin of the fragment cloud based on the concept that all fragments of a single breakup continue to pass through the breakup point in inertial space each successive revolution but at different times. The approximate time of breakup is determined by backdating the state of each fragment and plotting the running values of three functions to be defined later. The three functions define the approximate breakup time. A more definitive time as well as the location (latitude and longitude) of the breakup is then obtained by noting that most of the orbital planes of the fragments will have a slight inclination with respect to each other. However all of these planes intersect in a common line passing through the breakup point. This line is preserved for all time in inertial space except for perturbations. Using the approximate time already obtained, the effects of perturbations are minimized and the common line is determined which then defines a more precise time and location of the breakup.

The numerical procedure just described requires the orbits of individual fragments and consequently necessitates a large amount of computation. An alternative approach is to derive statistical characteristics of the ensemble without recourse to computation of individual orbits. This is accomplished by applying the methods of statistical mechanics. The structure of the cloud is calculated from its phase-space distribution function. This distribution function satisfies a first-order, linear partial differential equation, and Liouville's theorem states that it is an integral of the motion if the dynamical system is conservative. An analytic expression for the spatial density of the fragments can be found and used to determine the characteristics and the origin of the breakup.

THE DETERMINATION OF THE BREAKUP POINT

Conceptually the determination of the breakup point of a cloud of fragments may appear easy. One attempts to backdate the position vector of each fragment until all occupy the same position simultaneously. In practice the situation is not so simple. Usually many of the fragment pairs will not appear to pass within several tens or hundreds of kilometers of each other. Also the time of closest approach for each pair is usually different. These difficulties arise for the following reasons:

- The early-state estimates for each fragment may contain significant uncertainties due to the small length of the data span over which the orbits were fit;

- The set of orbital elements may contain entries which are not part of the actual breakup in question;

- For low-altitude fragments a significant drag term is sometimes computed during the orbit determination process; that is, the coefficients n_1 and n_2 are determined in the equation for mean motion:

$$M = M_0 + n_0(t - t_0) + n_1(t - t_0)^2 + n_2(t - t_0)^3. \quad (1)$$

While the determination of n_1 (n_2 is usually not determined for short arcs) results in a better fit over the data span, the extrapolation of equation (1) outside this domain back to the breakup point may result in significant position errors.

The procedure to be described is designed to minimize the effects of these problems and is guided by the following fundamental concepts:

- All fragments of a single orbital breakup occupy one point in space at one time only, this being the breakup place and time;

- Except for perturbations all fragments continue to pass through this point in inertial space each successive revolution but at different times.

A dual time-dependent and time-independent analysis is carried out. First an attempt is made to see if all the fragments can be backdated simultaneously to an approximate single point in time and space. Second an attempt is made to recover this point in inertial space independent of time.

The Time-Dependent Procedure

The procedure used to determine the approximate time of breakup is as follows: the state vectors of each fragment are simultaneously backdated, during which a running tabulation of three arbitrary functions of these positions is plotted. These functions are designed so as to peak in value whenever all or part of the fragment cloud has converged to an approximate point.

The first of the three functions is

$$F_1 = \sum_{i \neq j}^{n} \frac{1}{|\mathbf{r}_i - \mathbf{r}_j|^2 + \delta^2}, \tag{2}$$

where $\mathbf{r}_i$ and $\mathbf{r}_j$ are the position vectors to the ith and jth fragment respectively, n is the total number of fragments, and δ is a measure of the position uncertainty of the predicted positions $\mathbf{r}_i$ and $\mathbf{r}_j$. The uncertainty measure δ is set to 10 kilometers and is included to restrain F_1 from becoming infinite due to a single arbitrary close approach. Since the value of F_1 is insensitive to fragments which are not part of the breakup, the peaking of F_1 is a necessary but not sufficient condition that a breakup has occurred. F_1 is useful to determine the convergence of separate subclusters which may or may not occur at different times.

The second of the three functions is

$$F_2 = \frac{1}{\sum_{i \neq j}^{n} |\mathbf{r}_i - \mathbf{r}_j|^2}. \tag{3}$$

If the entire cluster size becomes small, the denominator in Eq. (3) will become small, resulting in a large positive value for F_2. However, since F_2 is greatly diminished in value for any one $|\mathbf{r}_i - \mathbf{r}_j|$ that does not become small, the maximization of F_2 is a sufficient condition to indicate a breakup.

The third of the three functions is

$$F_3 = \text{number of pairs such that } |\mathbf{r}_i - \mathbf{r}_j| \leqslant d_1, \tag{4}$$

where d_1 denotes an arbitrary distance ($\approx$100 km). F_3 therefore gives a measure of the number of close approaches within the distance d_1. The peaking of F_3 like F_1 is a necessary condition of a breakup. F_3 is used in conjunction with F_1 to eliminate false explosion times.

The Psuedo Time-Independent Determination

It is reasonable to assume that as a result of a satellite breakup most of the fragments will be given an out-of-plane velocity increment with respect to the parent satellite. The orbital inclinations of each fragment will thus be slightly different but will all intersect in a common line passing through the breakup point (Fig. 1). Except for perturbations this line is preserved in inertial space for all time. However due to oblateness the orbital planes of the fragments regress at slightly different rates because of the minor differences in their orbital periods and inclinations. Therefore, if the approximate time of the explosion is known and the orbital-plane intersections are calculated for each fragment pair, the explosion point in inertial space should be determined. Actually the line of intersections together with the orbital radius define two points in space. But it will seem later that although the out-of-plane component of the position distribution is zero

each half revolution from the breakup point, the radial component becomes zero each whole revolution. Therefore in principle the extraneous point can be eliminated.

Let $\mathbf{r}_i(t)$ and $\mathbf{v}_i(t)$ be the position and velocity vectors at time t of the ith fragment among n fragments. At any time t calculate the normal to the orbit plane:

$$\mathbf{h}_i(t) = \mathbf{r}_i \times \mathbf{v}_i, \quad i = 1, 2, \ldots, n . \tag{5}$$

Then calculate the line of intersection for each pair of orbital planes (Fig. 1):

$$\underset{i \neq j}{\mathbf{N}'_{i,j}} = \frac{\mathbf{h}_i \times \mathbf{h}_j}{|\mathbf{h}_i \times \mathbf{h}_j|}, \quad i, j = 1, 2, \ldots, n . \tag{6}$$

However each $\mathbf{N}'_{i,j}$ is expressed in inertial coordinates referenced to the true equator and equinox of date. The transformation to earth-fixed (rotating) coordinates is accomplished by

$$\begin{pmatrix} N_x \\ N_y \\ N_z \end{pmatrix} = \begin{pmatrix} \cos\gamma & \sin\gamma & 0 \\ -\sin\gamma & \cos\gamma & 0 \\ 0 & 0 & 1 \end{pmatrix} \mathbf{N}'_{i,j} , \tag{7}$$

where γ is the Greenwich hour angle, which is computed from the time given by the time-dependent analysis. The latitude φ and longitude λ of the intersection point are then given by

$$\underset{i \neq j}{\varphi_{i,j}} = \sin^{-1} N_z \tag{8}$$

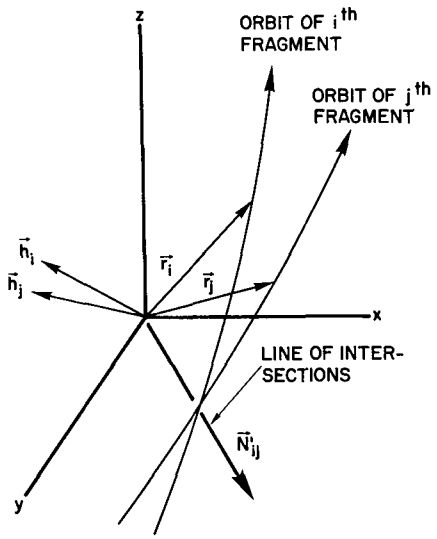

Fig. 1—Common intersection of orbit planes

and

$$\lambda_{\substack{i,j \\ i \neq j}} = \tan^{-1}\left(\frac{N_y}{N_x}\right). \tag{9}$$

Since many of the orbital-plane combinations will be nearly coplanar, their intersection lines will thus be poorly defined. Therefore only those plane intersections defining an angle greater than 1/10 degree will be considered physically meaningful. Any two fragments having a relative out-of-plane velocity of at least 12 m/s at the point of disintegration will meet this criterion.

The Analytical Prediction Scheme

The data on the individual fragments is provided in the form of mean elements by both NORAD and NAVSPASUR. For accuracy it is advantageous to use the same orbit-prediction process as was employed in the original differential corrections. However in the interest of computational efficiency a suitable simplication of these procedures is usually sufficient to obtain a prediction accuracy of 10 km over 5 days. This is the accuracy requirement that was imposed for this study.

The orbital parameters of each fragment obtained by NAVSPASUR were fitted to the observations by a modified Brouwer scheme [6]. Although the use of this procedure would yield the most accurate state prediction over the data span, a simplified procedure (NAVSPASUR one-line format) was used here for computational efficiency [6]. Essentially the method includes only the long-period and secular terms involving J_2, with the short-period terms being omitted. Using this method a 15-kilometer position accuracy can be obtained up to 10 days from epoch.

The data supplied from NORAD was backdated using a similar scheme [7] and is mainly a simplification of the analytical series produced by Arsenault, Chaffee, and Kuhlman [8]. This series contains all the long-period and secular terms involving J_2 and J_3 as well as all the short-period terms due to J_2 not containing eccentricity as a factor. It represents a compromise between computational accuracy and efficiency.

SIMULATED RESULTS

It is of interest to determine the minimum accuracy necessary of the initial states to achieve a successful prediction of the breakup point. Therefore satellite disintegrations were simulated to determine the effects of noisy data in calculating a breakup point.

In an example of the simulations it was assumed that at the time of breakup the parent satellite was in the orbit having the following Keplerian elements:

semimajor axis $a = 7000.0$ km,
eccentricity $e = 0.0$,
inclination $i = 45.0$ degrees,

nodal angle Ω = 0.0 degrees,
argument of perigee ω = 0.0 degrees, and
mean anomaly M = 0.0 degrees.

Each component of velocity was given a small velocity increment of zero mean and 10 m/s standard deviation. Then each fragment was propagated to a random epoch up to 10 days after the breakup. Noise was again added to the states, and an attempt to recover the explosion point was carried out. The computation of the breakup point was made for three separate levels of state uncertainties.

Figure 2a shows the results of the time-dependent procedure for a state uncertainty of zero mean and 0.05% standard deviation which is superimposed on the state vectors of each fragment. Figure 2b shows the results for an uncertainty of 0.09%. For this particular simulated breakup it is apparent that the breakup point can be recovered for an uncertainty of 0.05% and possibly 0.09%, although in the latter case F_3 is at a maximum one revolution past the explosion time. It is apparent from Fig. 2c that an uncertainty of 0.16% is definitely beyond the maximum that can be tolerated. Naturally when the breakup is more violent (explosion velocities $\approx$ 100 m/s), a proportionally higher uncertainty can be tolerated. Figure 3 shows the time-independent analysis for the three uncertainties. The line of intersections for the individual fragment pairs is shown only for those having a mutual intersection angle of 0.1 degree or more. Figure 3c shows the results for the highest noise level. The spread appears to be about 4 to 5 degrees in latitude. It appears therefore that the approximate position of breakup can be recovered by the time-independent analysis even though the time-dependent analysis fails (Fig. 2c).

In the simulation no attempt was made to conserve the momentum of the explosion about the parent satellite, since in practice only the larger fragments can be observed after a breakup. Also, momentum is not conserved if the breakup is the result of a collision with an external device.

RECONSTRUCTION OF ACTUAL BREAKUPS

Data were received from NORAD on the ITOS-F rocket-body breakup. which was launched November 6, 1973, into a 1500-km-altitude orbit and disintegrated during late December 1973. The data on the resulting fragments were cataloged within several days of the breakup. The orbits of 12 fragments were analyzed, and the results are shown in Fig. 4. Time is increasing to the left, and the functions are shown peaking at nearly the same point, indicating the approximate time of breakup. The peaks are quite broad, which shows an uncertainty of approximately a quarter orbit on either side of the maxima. The results of the time-independent analysis are shown in Fig. 5, with the latitudes and longitudes of the most significant plane intersections being indicated. It is apparent that the breakup occurred between 30°S and 45°S latitude near 180°W longitude, and correlation of these results with those of Fig. 4 indicates the time of the breakup to be at 0908Z ± 3 min on December 28, 1973.

The Cosmos-699 disintegration which occurred in mid-April 1975 proved to be another interesting case for study. The orbits of 33 fragments were observed and cataloged by NAVSPASUR [6] during the several days following the event. This apparently was a

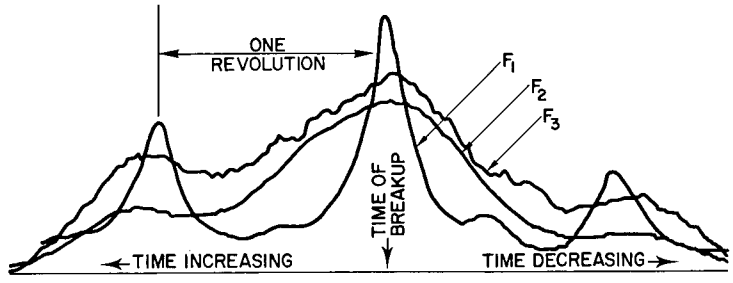

(a)—0.05% standard deviation

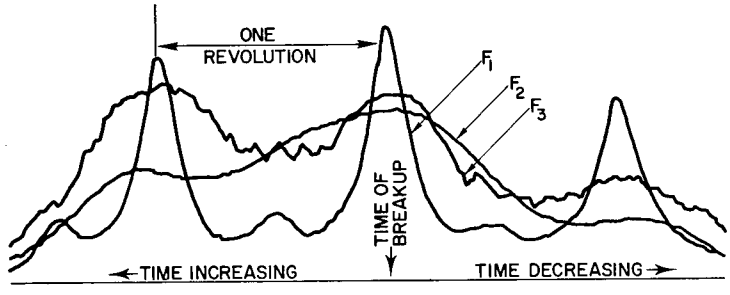

(b)—0.09% standard deviation

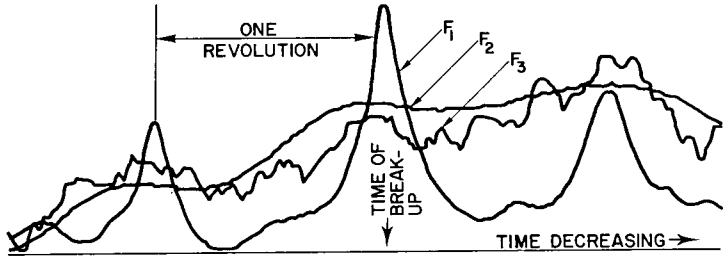

(c)—0.16% standard deviation

Fig. 2—Results of the time-dependent procedure using simulated data and state uncertainties with zero mean and various standard deviations

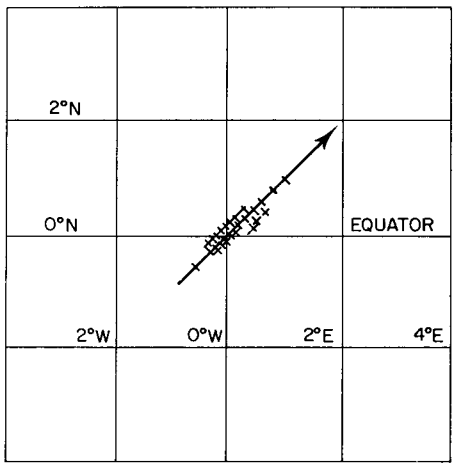

(a)—0.05% standard deviation

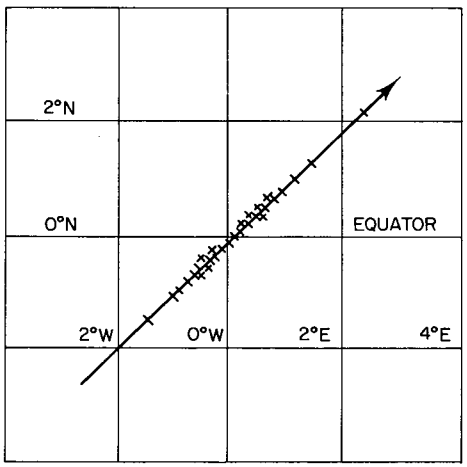

(b)—0.09% standard deviation

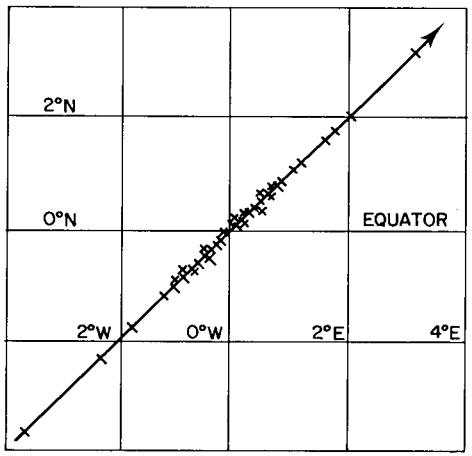

(c)—0.16% standard deviation

Fig. 3—Results of the time-independent procedure using simulated data and state uncertainties with zero mean and various standard deviations

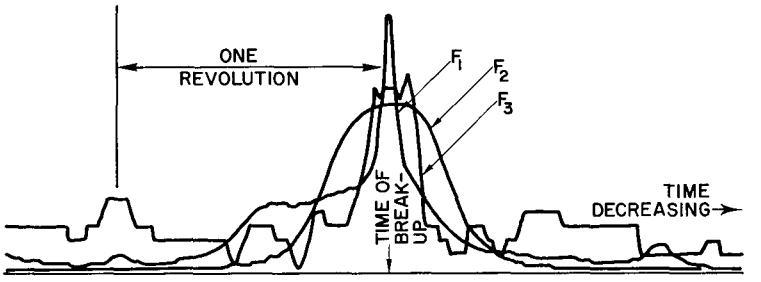

Fig. 4—Time-dependent analysis of ITOS-F rocket-body fragments

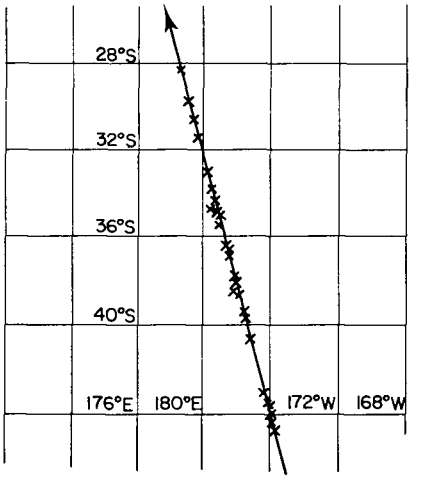

Fig. 5—Time-independent analysis of
ITOS-F rocket-body fragments

rather slow breakup. The velocity dispersion of the fragments appeared to be no more than 10 to 20 m/sec with respect to the cluster center, making a precise determination of the breakup time difficult. The results of the time-dependent study are shown in Fig. 6. F_1 shows a rather sharp peak, indicating at least a subset of the 33 fragments could be backdated to within a small cluster. F_2 and F_3 both show a rather broad peak due to the rather slow convergence of the total cluster. The three functions all indicate the approximate time of the breakup to be at 2147Z ± 5 min on April 17, 1975. The time-independent analysis is shown in Fig. 7. Due to the rather small velocity dispersion, few of the plane-intersection angles were greater than the desired 0.1 degree. Nevertheless this analysis shows the breakup point to be between 5°N, 83°W and 0°N, 81°W geocentric latitude and longitude. This confirms the results of the time-dependent analysis.

A rather violent breakup of the ERTS-I rocket body occurred on May 22, 1975, with over 100 fragments being cataloged by NORAD within several days of the breakup. The results of the time-dependent analysis is shown in Fig. 8. Due to the rather sharp peaking of both F_1 and F_2 the time of breakup is determined to within several minutes by this time-dependent procedure alone. The place and time of breakup are more

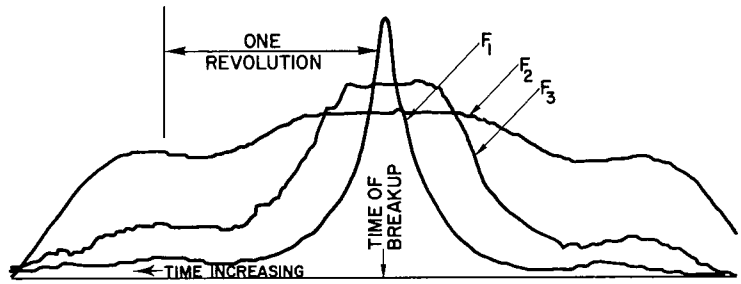

Fig. 6—Time-dependent analysis of COSMOS-699 fragments

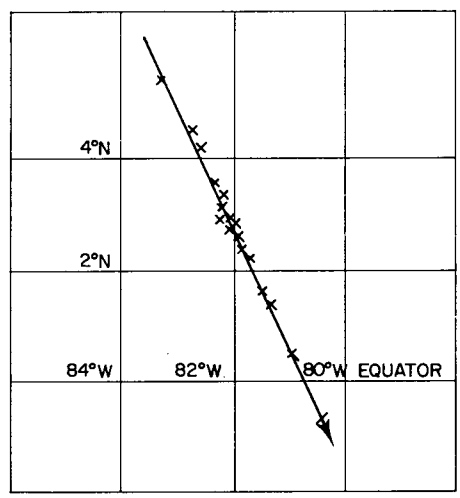

Fig. 7—Time-independent analysis of
COSMOS-699 fragments

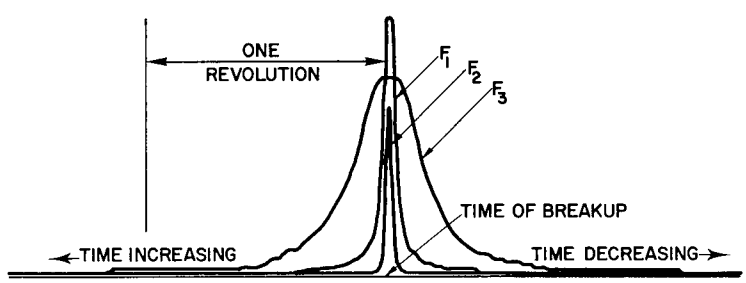

Fig. 8—Time-dependent analysis of ERTS-I rocket-body fragments

precisely determined by the time-independent procedure (Fig. 9), since the orbit-plane intersection angles are nearly 2 degrees for some fragment pairs. In Fig. 9 the spread in position is less than 0.5 degree. The location of the breakup is over 33.3°S geocentric latitude and 45.1°E longitude at 1827Z on May 22, 1975.

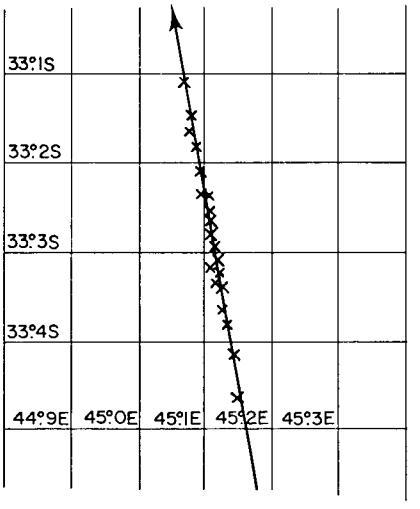

Fig. 9—Time-independent analysis of ERTS-I rocket-body fragments

The dispersion of the ERTS-I rocket-body fragment cloud from the time of breakup to 1/2 orbit later is shown in Fig. 10. Figures 10a through 10f show the evolution of the radial and downtrack component of the cloud. For these figures a simultaneous elongation and rotation of the fragment cloud is apparent. Figures 10g through 10l show the radial and crosstrack components of the cloud over the same time span. Note that one-half revolution from the breakup point the crosstrack component is nearly zero.

APPLICATION OF STATISTICAL MECHANICS

As mentioned in the Introduction, there are at least two methods for studying satellite breakups. The first, and historically the most common, is the study of trajectories of individual particles. The second method concentrates from the beginning on the statistical properties of the ensemble and seeks to derive them without recourse to large number of individual trajectories.

We shall investigate the second approach and apply methods of statistical mechanics to the problem. The technique we shall use is called the *continuum approach* in stellar dynamics [9]. However, the present problem is vastly less complicated than the problems of stellar dynamics, because we can ignore mutual interactions of the particles. The mathematical import is that we need appeal only to the well-developed theory of linear, first-order partial differential equations to obtain a solution.

The dispersion problem has two aspects, which we shall refer to as the *direct problem* and the *inverse problem.* In the direct problem one seeks to determine the fate of the ensemble from a priori knowledge of its origin. An example of the direct problem

would be the simulation of a satellite explosion. In the inverse problem one seeks to determine conditions at the origin from observations of the ensemble at a later time. The preceding studies of estimated satellite breakup times (involving Figs. 2, 4, 6, and 8) and positions at breakup (involving Figs. 3, 5, 7, and 9) are examples of the inverse problem.

Aside from the large literature on related problems in stellar dynamics and plasma physics, little attention has been given to the problem addressed here. A notable exception is an unpublished preprint by Langebartel [10], who applies the Liouville equation to the dispersion of particles in Hamiltonian systems and shows the utility of introducing generalized functions into the analysis. The four following subsections generalize and extend Langebartel's preprint (and have been submitted as a paper to *Astrophysics and Space Science* [11]). A good physical explanation of the dispersion of particles from orbiting, rotating artificial satellites is available in a paper by Ross [3].

Mathematical Formulation and Formal Solution

Consider an ensemble of non-interacting particles moving in a common force field such that the equations of motion for an individual particle are

$$\dot{\mathbf{q}} = \mathbf{X}(\mathbf{q}, \mathbf{p}, t) \tag{10a}$$

and

$$\dot{\mathbf{p}} = \mathbf{Y}(\mathbf{q}, \mathbf{p}, t) \tag{10b}$$

where the n-dimensional vectors $\mathbf{q}$ and $\mathbf{p}$ are the coordinates and momenta respectively. Let $f(\mathbf{q}, \mathbf{p}, t)$ be the phase-space density function for the ensemble such that a volume $d\mathbf{q}d\mathbf{p}$ at point $\mathbf{q}$, $\mathbf{p}$ contains dN particles at time t, where

$$dN = f(\mathbf{q}, \mathbf{p}, t)\, d\mathbf{q}d\mathbf{p} .$$

According to Chandrasekhar [12] the distribution function f satisfies the first-order, linear partial differential equation

$$\frac{\partial f}{\partial t} + \sum_{i=1}^{n} \left[\frac{\partial}{\partial q_i} (f X_i) + \frac{\partial}{\partial p_i} (f Y_i) \right] = 0 \tag{11}$$

if no source of particles is present. Equation (11) may be written

$$\frac{Df}{Dt} = -f\Delta , \tag{12}$$

where D/Dt denotes the "Stokes derivative"

$$D/Dt = \partial/\partial t + \mathbf{X} \cdot \nabla_{\mathbf{q}} + \mathbf{Y} \cdot \nabla_{\mathbf{p}}$$

and

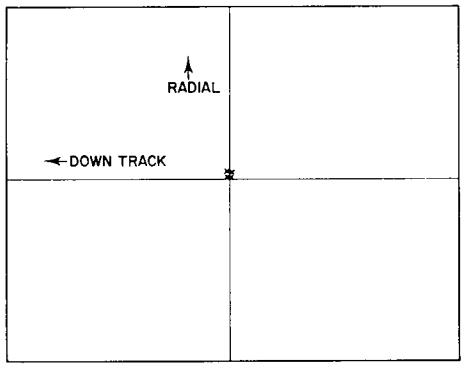

(a)—At the time of breakup

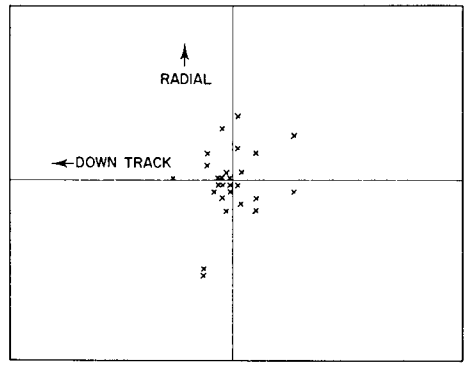

(d)—75 degrees after breakup

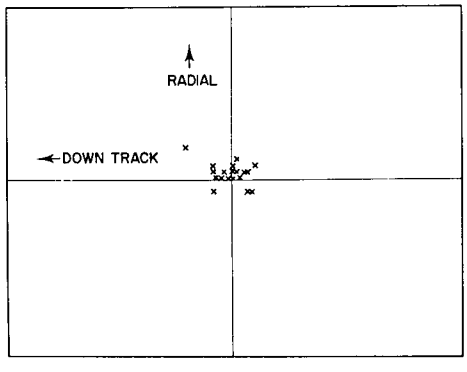

(b)—25 degrees after breakup

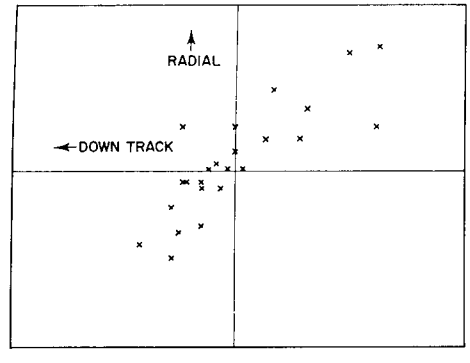

(e)—125 degrees after breakup

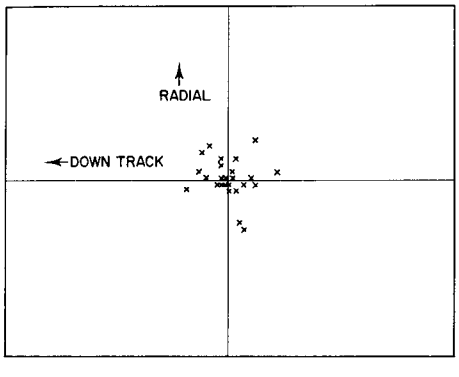

(c)—50 degrees after breakup

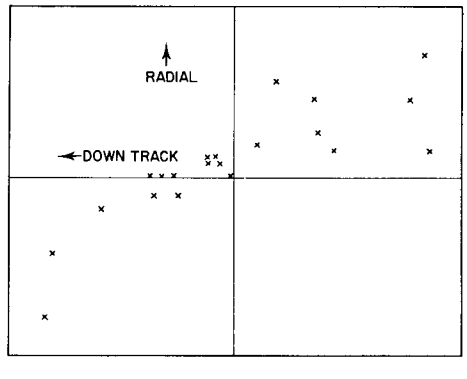

(f)—180 degrees after breakup

Fig. 10—Fragment positions of ERTS-I rocket body

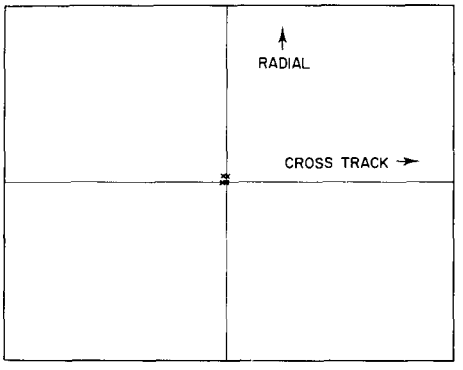

(g)—At the time of breakup

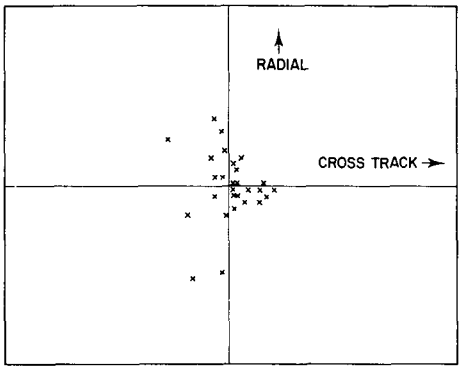

(j)—75 degrees after breakup

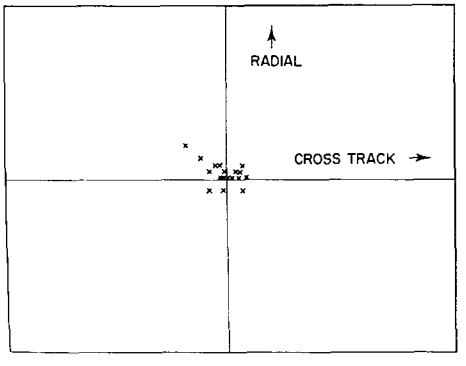

(h)—25 seconds after breakup

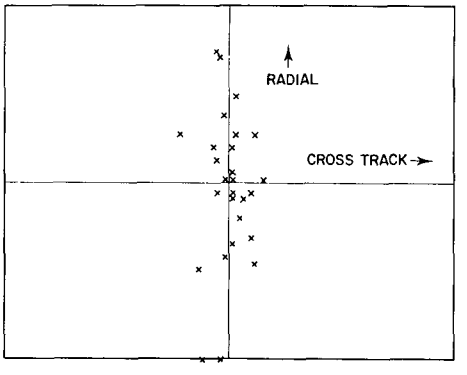

(k)—125 degrees after breakup

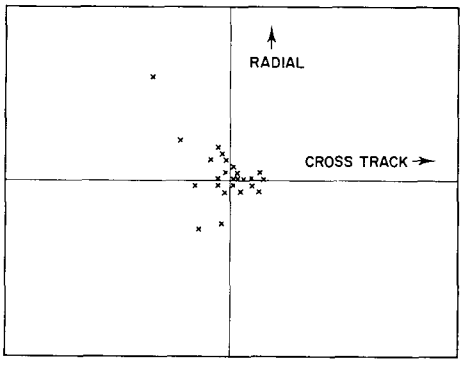

(i)—50 degrees after breakup

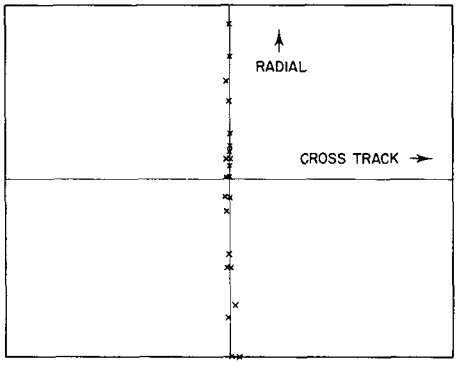

(l)—180 degrees after breakup

Fig. 10—Fragment positions of ERTS-I rocket body—Continued

$$\Delta = \sum_{i=1}^{n} \left[\frac{\partial X_i}{\partial q_i} + \frac{\partial Y_i}{\partial p_i} \right].$$

Given a particle at point $\mathbf{q}$, $\mathbf{p}$ in phase space at time t, let $\mathbf{Q}_0(q, p, t)$, $\mathbf{P}_0(q, p, t)$ denote its position at time $t = 0$. Similarly, for a particle at point $\mathbf{q}$, $\mathbf{p}$ at time $t = 0$, let $\mathbf{Q}(\mathbf{q}, \mathbf{p}, t)$, $\mathbf{P}(\mathbf{q}, \mathbf{p}, t)$ denote its position at time t. These functions are inverses of one another in the sense that

$$\mathbf{Q}_0[\mathbf{Q}(\mathbf{q}, \mathbf{p}, t), \mathbf{P}(\mathbf{q}, \mathbf{p}, t), t] = \mathbf{q}, \mathbf{P}_0[\mathbf{Q}(\mathbf{q}, \mathbf{p}, t), \mathbf{P}(\mathbf{q}, \mathbf{p}, t), t] = \mathbf{p} \tag{13a}$$

and

$$\mathbf{Q}[\mathbf{Q}_0(\mathbf{q}, \mathbf{p}, t), \mathbf{P}_0(\mathbf{q}, \mathbf{p}, t), t] = \mathbf{q}, \mathbf{P}[\mathbf{Q}_0(\mathbf{q}, \mathbf{p}, t), \mathbf{P}_0(\mathbf{q}, \mathbf{p}, t), t] = \mathbf{p}. \tag{13b}$$

The formal solution of (12) which satisfies the initial condition

$$f(\mathbf{q}, \mathbf{p}, 0) = F(\mathbf{q}, \mathbf{p}) \tag{14}$$

may now be written as

$$f(\mathbf{q}, \mathbf{p}, t) = F[\mathbf{Q}_0(\mathbf{q}, \mathbf{p}, t), \mathbf{P}_0(\mathbf{q}, \mathbf{p}, t)]\, e^{-\Gamma(\mathbf{q}, \mathbf{p}, t)}, \tag{15}$$

where

$$\Gamma(\mathbf{q}, \mathbf{p}, t) = \int_0^t \Delta[\mathbf{q}(t), \mathbf{p}(t), t]\, dt \tag{16}$$

and it is understood that the integral (16) is to be evaluated along the trajectory passing through $\mathbf{q}$, $\mathbf{p}$ at time t.

The spatial density $\rho(\mathbf{q}, t)$ is a fundamental descriptor of the ensemble of particles. It is obtained by integrating f over all momenta:

$$\rho(\mathbf{q}, t) = \int f(\mathbf{q}, \mathbf{p}, t) d\mathbf{p}. \tag{17}$$

The spatial density specifies the apparent shape and dispersion of the particle cloud at any time. The quadrature (17) is easily performed formally if the particles emanate from a common point.

To describe dispersion from a common point $\mathbf{q}_*$, we may use the initial condition

$$F(\mathbf{q}, \mathbf{p}) = \delta(\mathbf{q} - \mathbf{q}_*) G(\mathbf{p}), \tag{18}$$

where δ denotes the Dirac delta function and G is an arbitrary function which specifies the initial distribution of momenta.

We will evaluate the integral (17) by applying two theorems from the calculus of δ functions [13]:

$$\delta(\mathbf{x} - \mathbf{x}_0) = \delta(x_1 - x_{1,0})\delta(x_2 - x_{2,0}) \ \ldots \ \delta(x_n - x_{n,0}) \qquad \text{(Theorem I)}$$

and

$$\int \delta[\psi_1(\mathbf{x})]\,\delta[\psi_2(\mathbf{x})] \ \ldots \ \delta[\psi_n(\mathbf{x})]F(\mathbf{x})\,d\mathbf{x} = \frac{1}{|J|}F(\mathbf{x}_*), \qquad \text{(Theorem II)}$$

where $\mathbf{x}_*$ is determined from the equations

$$\psi_i(\mathbf{x}_*) = 0, i = 1, \ldots, n,$$

and J is the Jacobian determinant

$$J = \frac{\partial(\psi_1, \psi_2, \ldots, \psi_n)}{\partial(x_1, x_2, \ \ldots, x_n)}$$

evaluated at $\mathbf{x} = \mathbf{x}_*$. Theorem I relates a multidimensional δ function to the product of one-dimensional δ functions, and theorem II specifies the behavior of δ functions under a change of variable.

We substitute (18) and (15) into (17) to obtain

$$\rho(\mathbf{q}, t) = \int \delta[\mathbf{Q}_0(\mathbf{q}, \mathbf{p}, t) - \mathbf{q}_*]\,G[\mathbf{P}_0(\mathbf{q}, \mathbf{p}, t)]\,e^{-\Gamma(\mathbf{q}, \mathbf{p}, t)}d\mathbf{p}. \tag{19}$$

According to Theorems I and II we then obtain

$$\rho(\mathbf{q}, t) = \frac{1}{J}G[\mathbf{P}_0(\mathbf{q}, \mathbf{p}_*, t)]\,e^{-\Gamma(\mathbf{q}, \mathbf{p}_*, t)} \tag{20}$$

where $\mathbf{p}_*$ is the solution of the equation

$$\mathbf{Q}_0(\mathbf{q}, \mathbf{p}_*, t) = \mathbf{q}_* \tag{21}$$

and

$$J = \frac{\partial(Q_{0,1} \ \ldots \ Q_{0,n})}{\partial(p_1, \ldots, p_n)}. \tag{22}$$

Thus the calculation of the evolution of spatial density is reduced to the evaluation of a Jacobian determinant (22) and the solution of an equation (21) which is usually transcendental. The determinant involved is that of a submatrix of the matrizant of the variational

equations associated with the system (10) [14]. The matrizants for many dynamical systems are available in the literature. For example the matrizant for two-dimensional Keplerian motion is available in Deprit and Deprit-Bartholeme [15] and for three-dimensional Keplerian motion in Goodyear [16]; and methods for calculating matrizants for perturbed Keplerian motion are discussed by Danby [17] and Goodyear [18]. Equation (21) is also a generalization of a problem with a long tradition in celestial mechanics. For Keplerian motion it becomes a statement of Lambert's problem.

Liouville's theorem [19] asserts that $\Delta(\mathbf{q}, \mathbf{p}, t) \equiv 0$ for Hamiltonian dynamical systems. Hamiltonian systems then admit the simplification of setting to unity the exponential factor in equation (20). It is possible that $\Delta(\mathbf{q}, \mathbf{p}, t) = 0$ for a non-Hamiltonian system also.

The formal solution, as it stands, reveals little information about the physical behavior of dispersing ensembles of particles. To obtain more details and hence more physical insight, we now turn to specific systems. Linear systems admit a compact, explicit solution and will be treated in the next subsection. The subsequent subsection treats an especially important linear case: the case of small departures from circular orbits in an axially symmetric gravitational field.

The Variational Equations

Oftentimes dispersing systems have the property that the relative velocities of the particles are small in comparison with the total velocity of a reference particle at the time of disintegration. In these cases, one can profitably use the variational equations of the dynamical system to study the initial dispersion. The mathematics is considerably simplified in this case, because the equations become linear and, as mentioned, the matrizants for several important dynamical systems are available in the literature.

We now consider $\mathbf{q}$, $\mathbf{p}$ to be departures from a reference solution of system (10). The equations of motion for $\mathbf{q}$, $\mathbf{p}$ are the variational equations

$$\begin{pmatrix} \dot{\mathbf{q}} \\ \dot{\mathbf{p}} \end{pmatrix} = A \begin{pmatrix} \mathbf{q} \\ \mathbf{p} \end{pmatrix}, \tag{23}$$

where

$$A = \left(\begin{array}{c|c} A_{11} & A_{12} \\ \hline A_{21} & A_{22} \end{array}\right),$$

which is matrix of partial derivatives

$$A_{11} = \frac{\partial \mathbf{X}}{\partial \mathbf{q}}, \quad A_{12} = \frac{\partial \mathbf{X}}{\partial \mathbf{p}}, \quad A_{21} = \frac{\partial \mathbf{Y}}{\partial \mathbf{q}}, \quad \text{and } A_{22} = \frac{\partial \mathbf{Y}}{\partial \mathbf{p}}$$

to be evaluated on the reference solution.

The solution of the variational equations involves the matrizant

$$\Phi = \left(\begin{array}{c|c} U & V \\ \hline W & Y \end{array}\right),$$

where

$$U = \frac{\partial \mathbf{q}}{\partial \mathbf{q}_0}, \quad V = \frac{\partial \mathbf{q}}{\partial \mathbf{p}_0}, \quad W = \frac{\partial \mathbf{p}}{\partial \mathbf{q}_0}, \quad Y = \frac{\partial \mathbf{p}}{\partial \mathbf{p}_0},$$

and may be written

$$\begin{pmatrix} \mathbf{q} \\ \mathbf{p} \end{pmatrix} = \Phi \begin{pmatrix} \mathbf{q}_0 \\ \mathbf{p}_0 \end{pmatrix}, \tag{25}$$

where $\mathbf{q}_0$ and $\mathbf{p}_0$ are the initial values. If we adopt the notation that for any matrix $M(t)$

$$M\_(t) = M(-t),$$

then a fundamental property of matrizants may be written [14]

$$\Phi^{-1} = \Phi\_. \tag{26}$$

Equations (25) and (26) imply

$$\begin{pmatrix} \mathbf{q}_0 \\ \mathbf{p}_0 \end{pmatrix} = \Phi\_ \begin{pmatrix} \mathbf{q} \\ \mathbf{p} \end{pmatrix}$$

and the propagator functions $\mathbf{Q}_0$ and $\mathbf{P}_0$ of equations (13) become

$$\mathbf{Q}_0(\mathbf{q}, \mathbf{p}, t) = U\_\mathbf{q} + V\_\mathbf{p} \tag{27}$$

and

$$\mathbf{P}_0(\mathbf{q}, \mathbf{p}, t) = W\_\mathbf{q} + Y\_\mathbf{p}. \tag{28}$$

The Jacobian determinant (22) becomes

$$J = \det V\_, \tag{29}$$

and equation (21) becomes the linear equation

$$U\_\mathbf{q} + V\_\mathbf{p}_* = \mathbf{q}_*, \tag{30}$$

whose solution is

$$\mathbf{p}_* = V_-^{-1}(\mathbf{q}_* - U_-\mathbf{q}) . \tag{31}$$

The exponential factor appearing in equation (20) may be simplified by appealing to general properties of variational equations. Differentiating the determinant of Φ, we obtain [20]

$$\frac{dL}{dt} = L \sum_{i=1}^{n} \left(\frac{\partial \dot{q}_i}{\partial q_i} + \frac{\partial \dot{p}_i}{\partial p_i} \right) , \tag{32}$$

where

$$L = \det \Phi .$$

However, according to (23), (32) may be written

$$\frac{dL}{dt} = L\Delta \tag{33}$$

or

$$\frac{d}{dt}(\ell n\, L) = \Delta . \tag{34}$$

Therefore we obtain the following replacement for the exponential factor:

$$e^{-\int \Delta dt} = L(0)/L(t) . \tag{35}$$

When the preceding results are assembled, spatial density function for this case may be expressed

$$\rho(\mathbf{q}, t) = \frac{\det \Phi(0)}{[\det \Phi(t)]\, |\det V_-|}\, G[(W_- - Y_-V_-^{-1}U_-)\mathbf{q} + Y_-V_-^{-1}\mathbf{q}_*] . \tag{36}$$

Here we should recall that $\mathbf{q}$ now represents the departure from a reference solution of the original system (10) and that for a Hamiltonian system $\det \Phi \equiv 1$ by Liouville's theorem.

To recapitulate, we have found that the spatial density function associated with small departures from a reference solution is constructed entirely from the matrizant of the system. Our next step, taken in the next subsection, is to exhibit $\rho(\mathbf{q}, t)$ for the specific case of dispersion from a circular orbit and to give an example of numerical results for this case.

Slow Dispersion from a Circular Orbit

Let us now consider the specific case of dispersion of particles from an object in a circular orbit in an axially symmetric gravitational field. We introduce cylindrical coordinates ϖ, θ, and z such that the plane $z = 0$ is a plane of symmetry of the gravitational field. The gravitational potential then depends only on ϖ and z:

$$\mathcal{V} = \mathcal{V}(\varpi, z) .$$

Such a potential admits circular orbits in the plane $z = 0$. A circular orbit of radius R is described parametrically by

$$\varpi = R,$$

$$\theta = \theta_0 + \Omega t,$$

and

$$z = 0,$$

where $R\Omega^2 = \partial\mathcal{V}/\partial\varpi(R, 0)$. Consider departures ξ, η, ζ from this reference orbit such that

$$\varpi = R + \xi, \tag{37a}$$

$$\theta = \theta_0 + \Omega t + \eta/R, \tag{37b}$$

and

$$z = \zeta. \tag{37c}$$

The variational equations for ξ, η, and ζ are generated from the Hamiltonian

$$\mathcal{H} = \frac{1}{2}(p_1^2 + p_2^2 + p_3^2) - 2\Omega\xi p_2 + \frac{1}{2}(n^2\xi^2 + K^2\zeta^2), \tag{38}$$

where the momenta are

$$p_1 = \dot{\xi}, \tag{39a}$$

$$p_2 = \dot{\eta} + 2\Omega\xi, \tag{39b}$$

and

$$p_3 = \dot{\zeta} \tag{39c}$$

and where

$$n^2 = 3\Omega^2 - \frac{\partial^2}{\partial \varpi^2} \mho\,(R, 0) \tag{40a}$$

and

$$K^2 = \frac{\partial^2}{\partial z^2} \mho\,(R, 0)\,. \tag{40b}$$

We will assume that n^2 (the square of the epicyclic frequency) and K^2 are positive, so that $\mho$ is stable to small departures from circular orbits.

If we introduce the notation

$\tau = nt,$

$\tau' = Kt,$

$\sigma = 2\Omega/n,$

$s = \sin \tau,$

$c = \cos \tau,$

$s' = \sin \tau',$

and

$c' = \cos \tau',$

then the fundamental matrices can be written

$$U = \begin{pmatrix} c & 0 & 0 \\ -\sigma s & 1 & 0 \\ 0 & 0 & c' \end{pmatrix}, \tag{41a}$$

$$V = \frac{1}{n}\begin{pmatrix} s & -\sigma(c-1) & 0 \\ \sigma(c-1) & (1-\sigma^2)\tau + \sigma^2 s & 0 \\ 0 & 0 & ns'/K \end{pmatrix}, \tag{41b}$$

$$W = \begin{pmatrix} -ns & 0 & 0 \\ 0 & 0 & 0 \\ 0 & 0 & -Ks' \end{pmatrix}, \tag{41c}$$

and

$$Y = \begin{pmatrix} c & \sigma s & 0 \\ 0 & 1 & 0 \\ 0 & 0 & c' \end{pmatrix} \tag{41d}$$

To complete the solution, we require

$$D \equiv \frac{K}{s'} \det V_- = (1 - \sigma^2)s\tau + 2\sigma^2(1 - c) \tag{42}$$

and

$$W_- - Y_- V_-^{-1} U_- = \begin{pmatrix} \frac{n}{D}[(1 - \sigma^2)\tau + \sigma^2 s] & -\frac{n}{D}\sigma(1 - c) & 0 \\ \frac{n}{D}\sigma(1 - c) & \frac{n}{D}s & 0 \\ 0 & 0 & \frac{K}{s'} \end{pmatrix}. \tag{43}$$

The explicit equation for the spatial density is then

$$\rho(\xi, \eta, \zeta, t) = \frac{K}{|s'[(1 - \sigma^2)s\tau + 2\sigma^2(1 - c)]|} G\left(\frac{n}{D}\{[(1 - \sigma^2)\tau + \sigma^2 s]\xi - \sigma(1 - c)\eta\}, \frac{n}{D}[\sigma(1 - c)\xi + s\eta], \frac{K}{s'}\zeta\right) \tag{44}$$

for any initial momentum distribution function $G(p_1, p_2, p_3)$.

To illustrate these results, a distribution function

$$G(\mathbf{p}) = e^{[(p_1 - 0.001)^2 + (p_2 - 0.001)^2 + p_3^2]/(0.003)^2} H(0.007 - \sqrt{p_1^2 + p_2^2}) H(0.007 - p_3)$$

with the Keplerian parameters $n = K = 1$ and $\sigma = 2$ was used to evaluate the spatial density function (44) at various times. The results are shown in Figs. 11a through 11f as a symbolic representation of the relative density. To produce two-dimensional figures, the density has been calculated in the reference orbit plane and in the principal plane of the cloud, which is normal to the reference orbit plane. The position of the reference body is always at the origin of the coordinate systems. The center of mass of the cloud executes an epicycle about the reference orbit and the cloud elongates and rotates to align itself with the direction of motion as time increases. There is a boundary $\rho = 0$ for each figure because of the Heaviside function $H(a - x)$ in the distribution function. The reference orbit plane is always a plane of symmetry for the cloud. The section by the reference plane (intersection of the cloud and the reference plane) collapses to a line once per revolution, and the section by the plane normal to the reference plane collapses to a line twice per revolution. Knowing that the salient features of the evolution of the cloud are its rotation and elongation, we may undertake the calculation of these quantities from the spatial density function (44). We will restrict our attention in this calculation to an ellipsoidal momentum distribution function G typified by the illustrative example (Fig. 11).

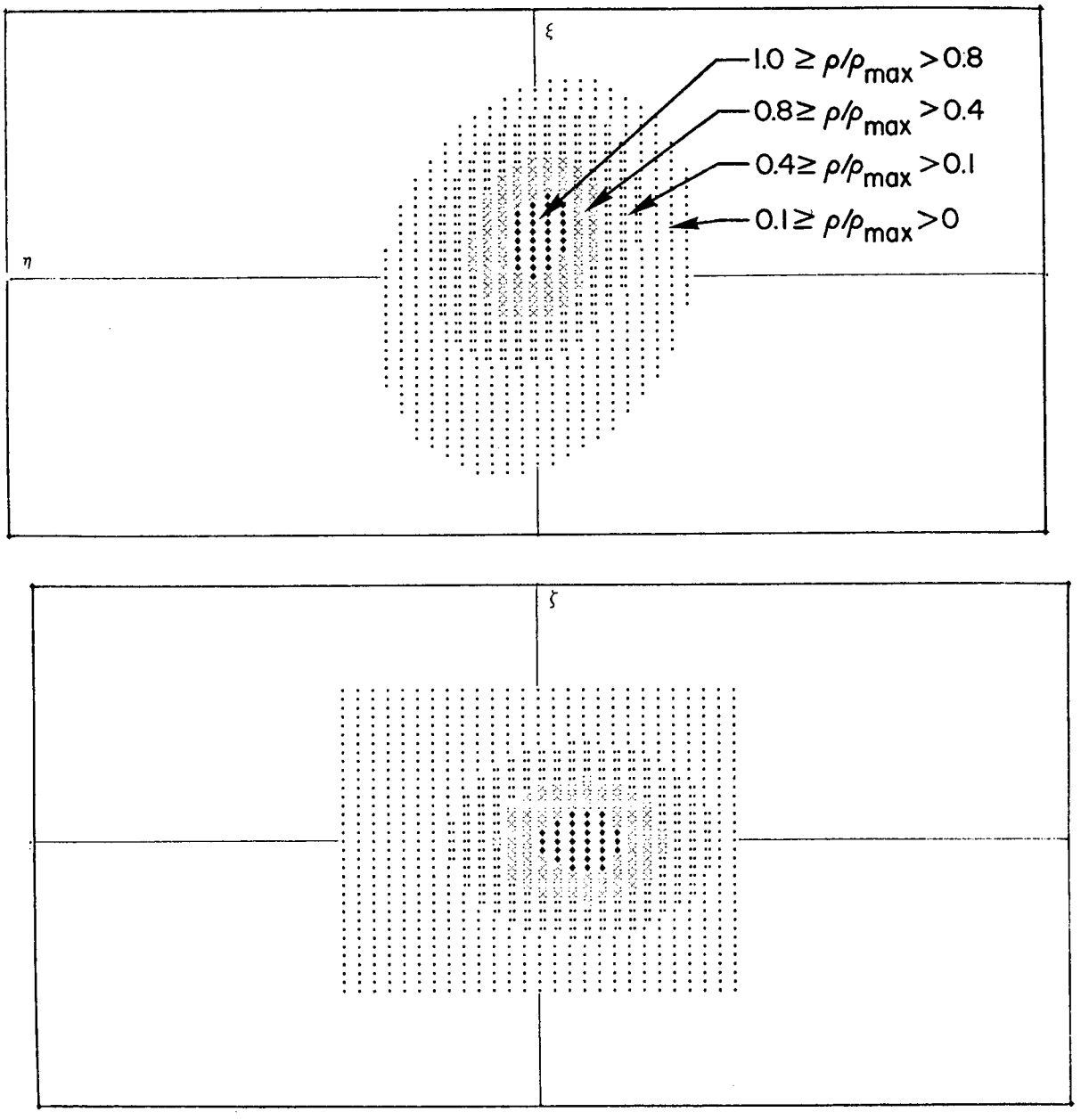

Fig. 11a—Symbolic representation of the relative spatial density at $\tau = \pi/4$ on (top) the reference orbit plane and (bottom) a plane normal to the reference orbit plane containing two principle axes.

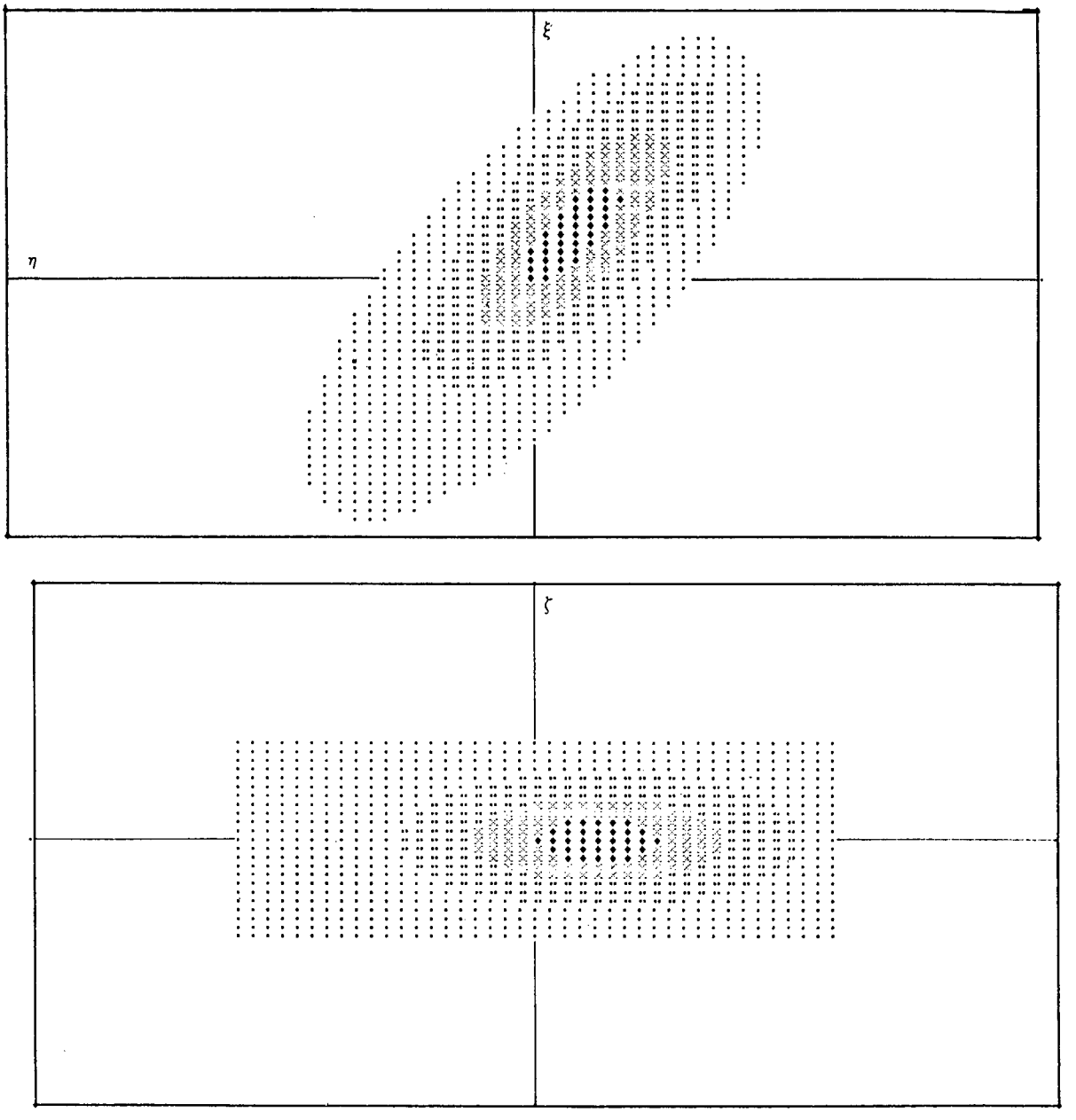

Fig. 11b—Relative spatial density at $\tau = \pi/2$, on a scale 1/2 that of Fig. 11a

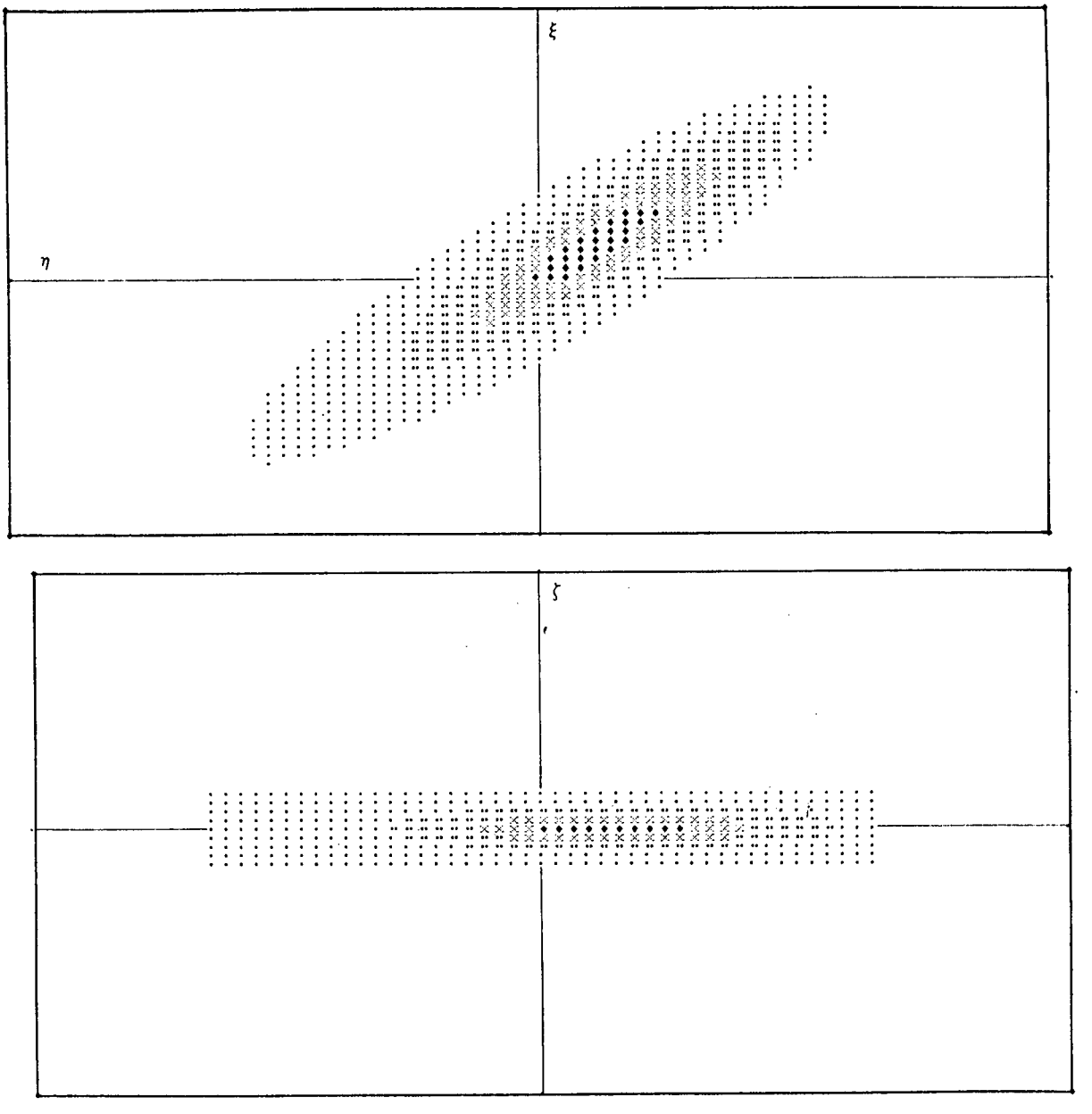

Fig. 11c—Relative spatial density at $\tau = 3\pi/4$, on a scale 1/4 that of Fig. 11a

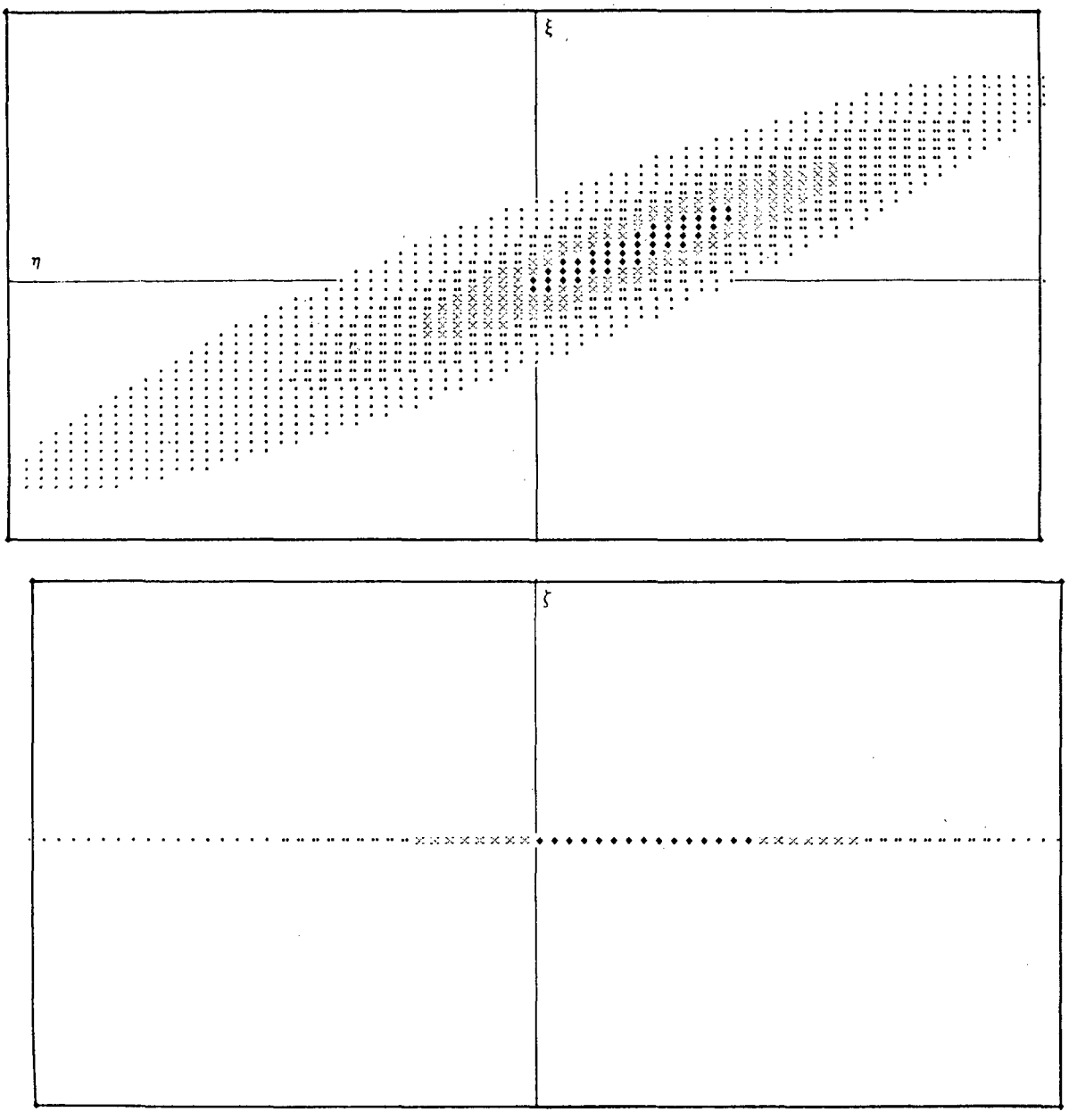

Fig. 11d—Relative spatial density at $\tau = \pi$, on a scale 1/4 that of Fig. 11a

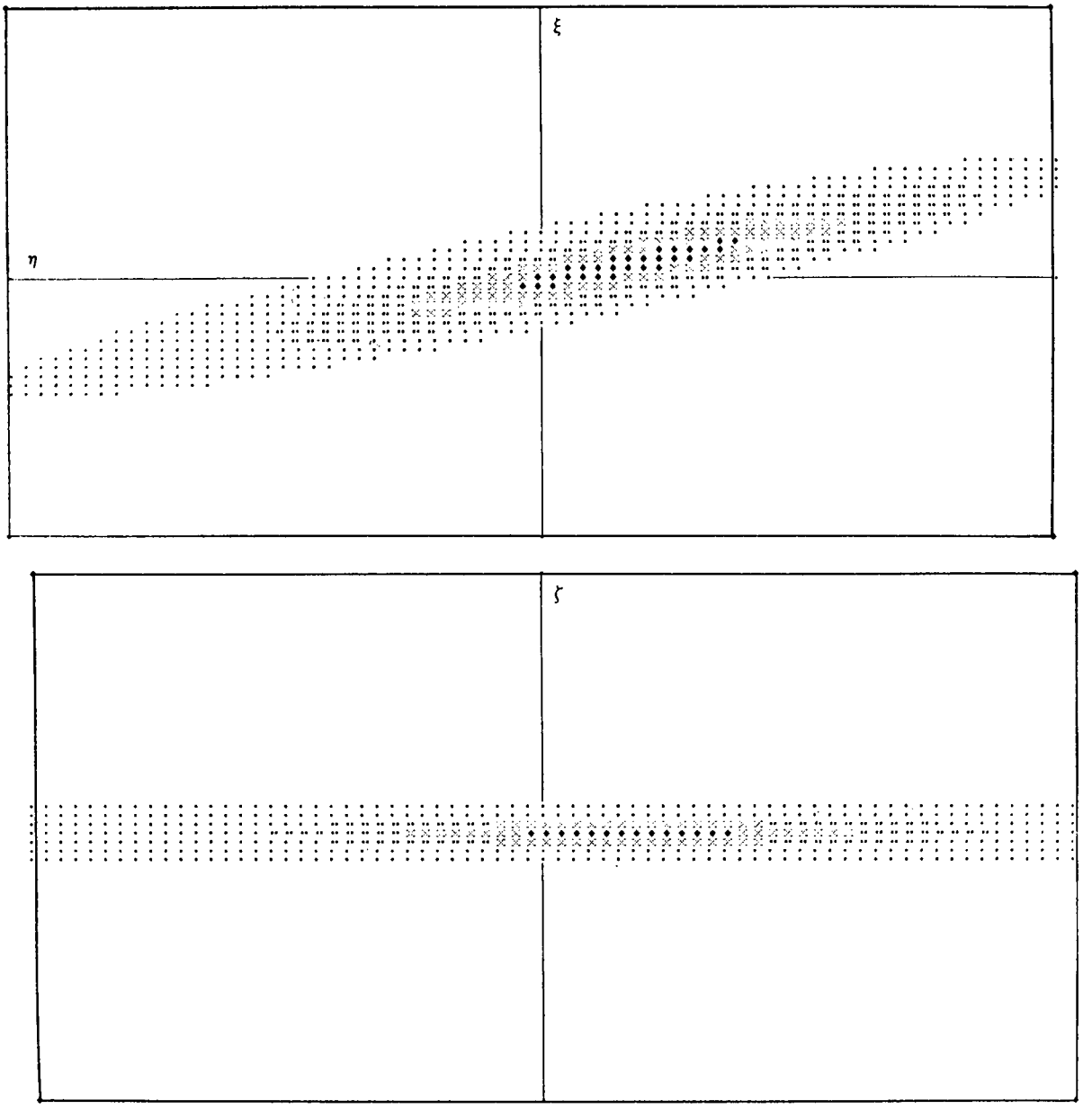

Fig. 11e—Relative spatial density at $\tau = 6\pi/4$, on a scale 1/6 that of Fig. 11a

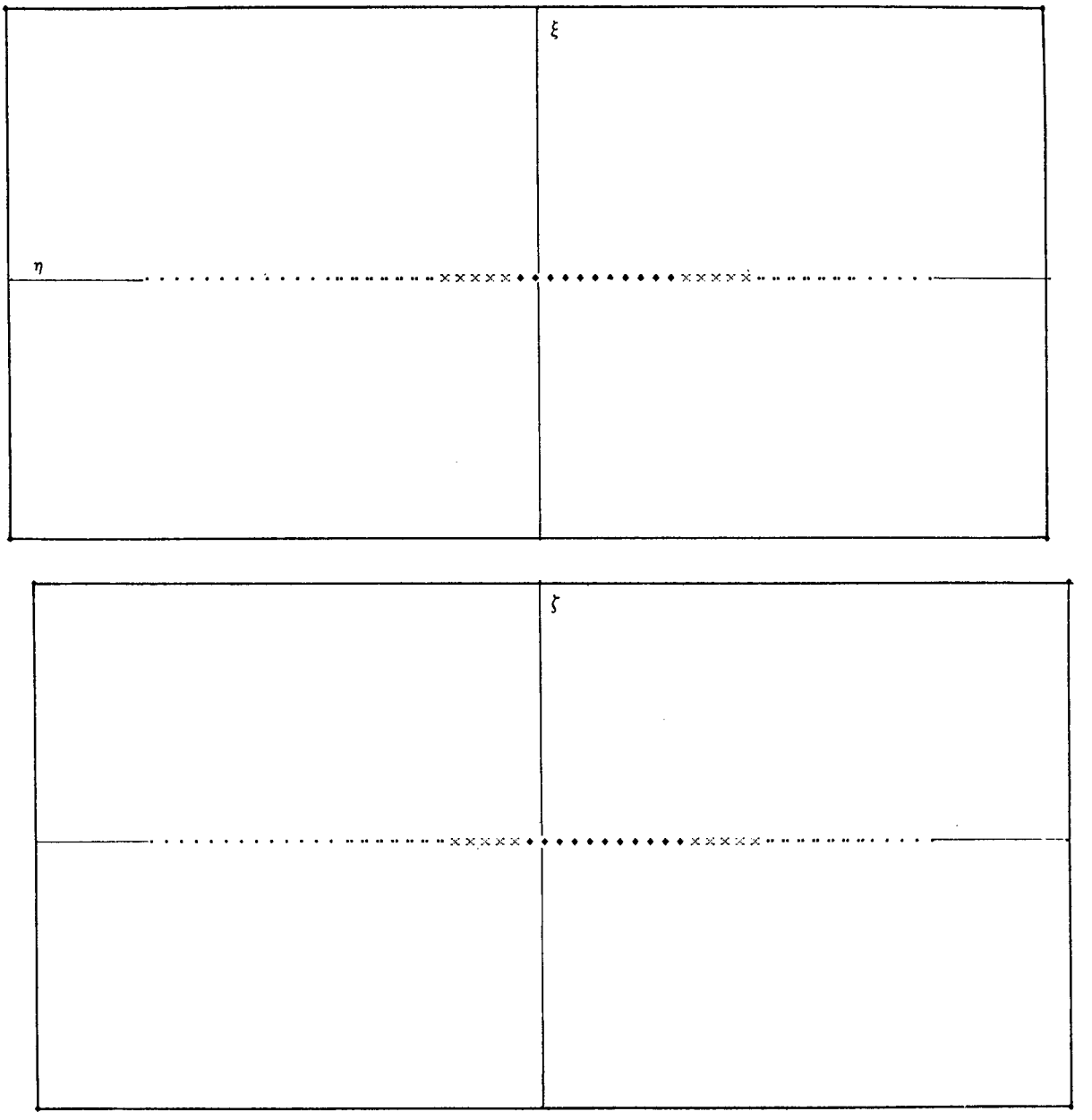

Fig. 11f—Relative spatial density at $\tau = 2\pi$, on a scale 1/10 that of Fig. 11a

Let

$$G(\mathbf{p}) = e^{-(\mathbf{p}-\beta)\cdot A(\mathbf{p}-\beta)}, \tag{45}$$

where A is the diagonal matrix

$$A = \text{diag}\,\{1/\alpha_1^2, 1/\alpha_2^2, 1/\alpha_3^2\}.$$

It follows immediately from (44) and (20) that the spatial density function is also ellipsoidal and that the maximum density (which is also the mean density in this case) occurs on the solution curve of (38) corresponding to the initial conditions $\mathbf{q} = 0$ and $\mathbf{p} = \beta$, that is, the epicycle corresponding to the mean of the initial momenta. This conclusion could also be reached by examining the first moments of $\rho(q, t)$ with respect to ξ, η, and ζ.

The out-of-plane structure of the ensemble, namely, its dependence on ζ, is independent of its in-plane structure. An ensemble with initial momentum distribution (45) is always oriented parallel to the orbit plane. A skewness relative to the orbit plane cannot develop unless it is present initially. The dispersion in the ζ direction is $\alpha_3 s'/K$, which shows that the ensemble collapses to the orbit plane when $s' = 0$ or $t = n\pi/K$, $n = 1, 2 \ldots$.

The orientation and elongation of the cloud may be determined by calculating the second moments of ρ about the mean with respect to the coordinates ζ and η. It is easier in this case however to diagonalize the quadratic form which appears in the exponent of equation (45). We find that the angle ω between the major axis of the ensemble and the ζ axis satisfies

$$\tan 2\omega = \frac{2\sigma(1-c)(s - [(1-\sigma^2)\tau + \sigma^2 s](\alpha_2/\alpha_1)^2)}{\sigma^2(1-c)^2 - s^2 + \{[(1-\sigma^2)\tau + \sigma^2 s]^2 - \sigma^2(1-c)^2\}(\alpha_2/\alpha_1)^2} \tag{46}$$

The major and minor axes a and b of the ellipse are found to satisfy

$$\begin{aligned} 1/b^2 \\ \text{or} \\ 1/a^2 \end{aligned} = \frac{1}{2}\left(\frac{[\sigma^2(1-c)^2 + s^2]}{\alpha_2^2} + \frac{[1-\sigma^2)\tau + \sigma^2 s]^2 + \sigma^2(1-c)^2}{\alpha_1^2}\right.$$
$$\left. \pm \frac{2}{\sin 2\omega}\left\{\frac{\sigma(1-c)s}{\alpha_2^2} - \frac{[(1-\sigma^2)\tau + \sigma^2 s]\sigma(1-c)}{\alpha_1^2}\right\}\right). \tag{47}$$

The orientation angle ω is seen to be completely determined by the ratio α_2/α_1 or, equivalently, by the eccentricity of the initial momentum ellipsoid, but determining the major and minor axes requires that the separate major and minor axes α_1 and α_2 of the initial momentum ellipsoid be determined. A family of curves of ω versus τ parameterized by $(\alpha_2/\alpha_1)^2$ is shown in Fig. 12a. The semimajor and semiminor axes versus time for the illustrative example are shown in Fig. 12b. Also shown in Fig. 12a (open circles) are orientation angles observed for the initial dispersion of the breakup of the artificial satellite Cosmos 699. Agreement is good between the observed values and the curve calculated for $\alpha_1 = \alpha_2$. Figure 12b shows that the ensemble elongates rapidly. This has an

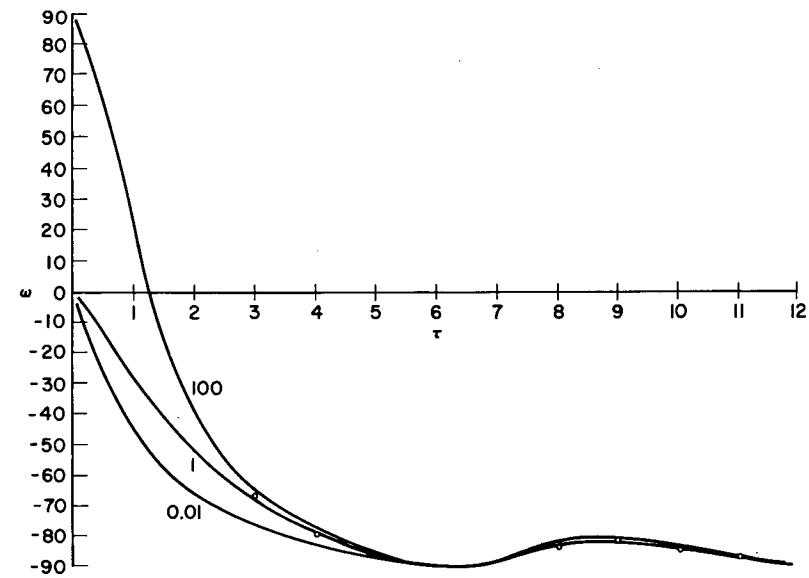

Fig. 12a—Orientation angle ω of the particle ensemble as a function of τ and parameterized by $(\alpha_2/\alpha_1)^2$, obtained using equation (46)

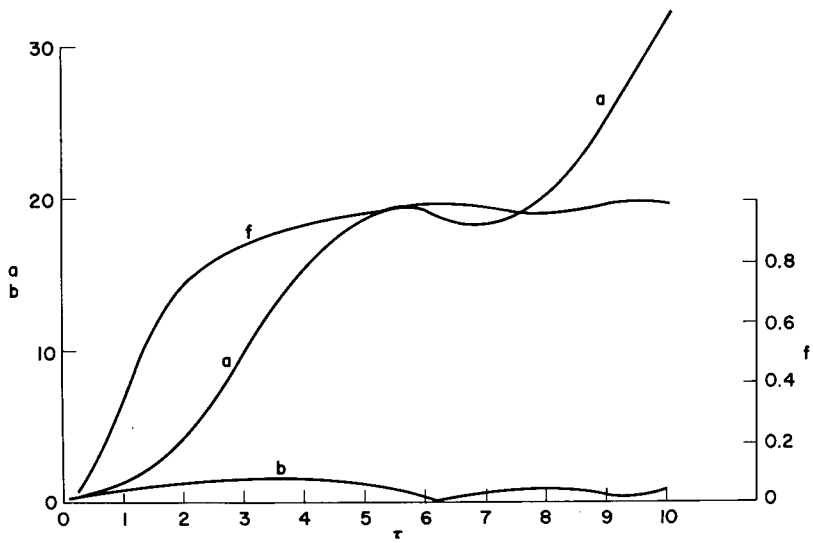

Fig. 12b—Semimajor and semiminor axes a and b, obtained using equation (47), and flattening f of the particle ensemble

important observational consequence. Any process of orbit determination has intrinsic uncertainties because of observation errors. The uncertainties can completely distort the structure near the point of disintegration but will be relatively inconsequential once the major axis of the ellipsoid has exceeded the uncertainties.

The Inverse Problem

We have seen that the extent and orientation of the ensemble can be calculated given the initial momentum distribution. Now we consider the inverse problem of determining the initial time and velocity distribution from knowledge of the ensemble structure at a later time. We give explicit results for the case of an elliposidal distribution of initial momenta and will indicate a numerical procedure for treating more general cases.

We consider the quadratic form Q which appears in the exponent of the distribution function G in equation (44) in the elliposidal case:

$$Q = I_{20}\xi^2 + 2I_{11}\xi\eta + I_{02}\eta^2 ,$$

where

$$I_{20} = \frac{n^2}{D^2}\left\{\frac{[(1-\sigma^2)\tau + \sigma^2 s]^2}{\alpha_1^2} + \frac{\sigma^2(1-c)^2}{\alpha_2^2}\right\} , \tag{48a}$$

$$I_{11} = \frac{n^2}{D^2}\left\{-\frac{[(1-\sigma^2)\tau + \sigma^2 s]}{\alpha_1^2} + \frac{s^2}{\alpha_2^2}\right\}\sigma(1-c), \tag{48b}$$

and

$$I_{02} = \frac{n^2}{D^2}\left[\frac{\sigma^2(1-c)^2}{\alpha_1^2} + \frac{s^2}{\alpha_2^2}\right] . \tag{48c}$$

The shape and orientation of the ellipsoid at time t determines I_{20}, I_{11}, and I_{02}, and these quantities are regarded as known. The parameters α_1 and α_2 determine the initial distribution and, along with t, are unknown. Thus equation (48) supply three equations in three unknowns. The equations are linear in $1/\alpha_1^2$ and $1/\alpha_2^2$, so these quantities are easily eliminated. The result is the following transcendental equation for τ (or t):

$$\det\begin{pmatrix} I_{20} & I_{11} & I_{02} \\ [(1-\sigma^2)\tau + \sigma^2 s]^2 & -\sigma(1-c)[(1-\sigma^2)\tau + \sigma^2 s] & \sigma^2(1-c)^2 \\ \sigma^2(1-c)^2 & \sigma(1-c)s & s^2 \end{pmatrix} = 0 \tag{49}$$

The roots of equation (49) are not simple, and further information is necessary to distinguish the correct one. This may be accomplished in one of two ways. First, equation (49) may be solved twice, for values of I_{ij} observed at two times separated by a known interval ΔT. The pair of roots differing by ΔT then determine the initial time τ. Second, the values of α_1 and α_2 can be calculated from

$$\det \begin{pmatrix} [(1-\sigma^2)\tau + \sigma^2 s]^2 & \sigma^2(1-c)^2 \\ \sigma^2(1-c)^2 & s^2 \end{pmatrix} \begin{pmatrix} 1/\alpha_1^2 \\ 1/\alpha_2^2 \end{pmatrix}$$

$$= \frac{n^2}{D^2} \begin{pmatrix} I_{20}s^2 - \sigma^2(1-c)^2 I_{02} \\ -\sigma^2(1-c)^2 I_{20} + [(1-\sigma^2)\tau + \sigma^2 s]^2 I_{02} \end{pmatrix} \tag{50}$$

at two times separated by a known ΔT. The pair of roots having the same associated values of ΔT then give the correct initial time. In either case the values of I_{ij} must be known at two different times in order to determine a unique solution.

The computational procedure is illustrated in Fig. 13 for the case $\sigma = 2$ (Keplerian motion) and $\alpha_1 = \alpha_2 = 1$. The two curves were calculated with $I_{20} = 0.428$ and 0.394, $I_{11} = 0.322$ and 0.259, $I_{02} = 0.512$ and 0.256, and $\Delta T = 0.5$. The origin of the lower curve is shifted so that the proper root is the one which aligns the intersections of the upper and the lower curves. Table 1 displays the associated values of $1/\alpha_1^2$ and $1/\alpha_2^2$ for the first two roots.

Table 1—Roots of Equation (49)

t	$1/\alpha_1^2$	$1/\alpha_2^2$
0.93	0.16	0.59
1.50	1.00	1.00
$0.76 + \Delta T$	0.12	0.77
$1.50 + \Delta T$	1.00	1.00

The computational procedure which we have illustrated for the ellipsoidal velocity distribution leads to the initial time and the initial distribution because it can be described completely by its first and second moments. In general, higher order moments will be required to determine the initial distribution and the initial time. For these cases one may evaluate the integrals

$$I_{ijk}(t) = \int \xi^i \eta^j \zeta^k \rho(\xi, \eta, \zeta, t)\, d\xi d\eta d\zeta \tag{51}$$

using equation (36) or equation (44) for $\rho(\xi, \eta, \zeta, t)$. The right-hand side may be expressed in terms of the initial moments $I_{ijk}(0)$. This relates the observed moments $I_{ijk}(t)$

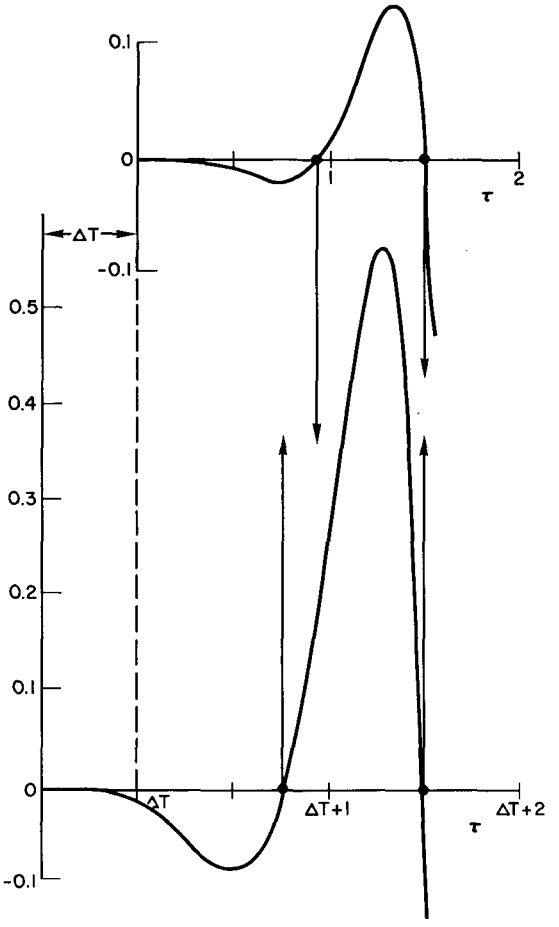

Fig. 13—Graphical solution of the inverse problem

on one hand to the initial moments $I_{ijk}(0)$ and the time t elasped since initial dispersion on the other. The details of this procedure are left for future work.

PROBABILITY OF COLLISION

The number of objects in orbit about the earth has increased enough that planners of manned missions must consider the hazard of collision with debris and/or payloads. A particularly hazardous situation occurs when objects such as fuel tanks or rocket bodies disintegrate and temporarily produce regions of anomalously high particle density. In this subsection, we consider the problem of calculating a probability of collision with a dispersing cloud of particles.

Our model of the dynamical system consists of a continuum of particles specified by a phase-space distribution function and a single reference particle whose trajectory is known with complete certainty. We desire to know the probability that a particle of the continuum shall pass within a given distance of the reference particle during a specified

interval of time. The given distance must be large enough that the hypothesis of zero uncertainty in the reference orbit is reasonable.

We shall first consider the problem in the abstract. A formal solution consists of a constructive definition of collision probability. The computation of this probability is another problem. In most cases extensive numerical work will be required. However, the case in which the continuum of particles represents an ensemble which is slowly dispersing from a known parent orbit can be treated semianalytically.

Let the particle continuum be described by a phase-space distribution function $f(\mathbf{q}, \mathbf{p}, t)$ as earlier. Let Π denote the phase space. The probability that a particle will be found in a region R at time t is

$$p(R, t) = \frac{1}{N} \int_R f(\mathbf{q}, \mathbf{p}, t)\, d\mathbf{q}\, d\mathbf{p}, \tag{52}$$

where

$$N = \int_\Pi f(\mathbf{q}, \mathbf{p}, t)\, d\mathbf{q}\, d\mathbf{p}.$$

If $\rho(q, t)$ is the spatial density function, we can likewise define the probability that a particle will be found in a subset $\mathcal{Q}$ of configuration space as

$$p_Q(\mathcal{Q}, t) = \frac{1}{M} \int_{\mathcal{Q}} \rho(\mathbf{q}, t)\, d\mathbf{q} \tag{53}$$

where

$$M = \int \rho(\mathbf{q}, t)\, d\mathbf{q}$$

and the integral is taken over all admissible configurations. The quantity p_Q can be regarded as a local or instantaneous measure of probability of collision but is not suitable for describing the probability over an extended interval of time. It can be calculated by numerical quadratures in a straightforward way using expressions for $\rho(\mathbf{q}, t)$ given before.

Formulation of a definition of collision probability over an extended time interval requires the introduction of some additional notation. Given a subset $\mathcal{S} \subseteq \Pi$, let

$$T_t \mathcal{S} = \{(\mathbf{q}, \mathbf{p}) \in \Pi\colon\ [\mathbf{Q}_0(\mathbf{q}, \mathbf{p}, t), \mathbf{P}_0(\mathbf{q}, \mathbf{p}, t)] \in \mathcal{S}\}, \tag{54}$$

where $\mathbf{Q}_0$ and $\mathbf{P}_0$ are the propagator functions (equations (13)). T_t specifies the evolution of a subset of initial conditions in Π. Let $\mathbf{q}_R(t)$, $\mathbf{p}_R(t)$ be the position in Π of the reference particle. Let $\mathcal{C}_\Delta(t) = \{(q, p)\colon\ |\mathbf{q} - \mathbf{q}_R(t)| < \Delta\}$. $\mathcal{C}_\Delta(t)$ consists of the

continuum particles lying within a distance Δ of the reference particle at time t, that is, those particles which "collide" with the reference particle.

We define the probability $p(\Delta, t)$ that a continuum particle will pass within a distance Δ of the reference particle in the time interval $(0, T)$ to be

$$p(\Delta, T) = \frac{1}{N} \int_{\mathcal{U}} f(\mathbf{q}, \mathbf{p}, 0)\, d\mathbf{q}\, d\mathbf{p}\,, \tag{55}$$

where

$$\mathcal{U} = \bigcup_{t \in (0,T)} T_{-t}\, \mathcal{C}_{\Delta}(t).$$

The subset $\mathcal{U} \subseteq \Pi$ consists of all initial conditions which lead to a collision in the time interval $(0, T)$. The idea then is to transfer everything back to the reference time $t = 0$ before evaluating the probability integral.

If the continuum particles emanate from a common point $\mathbf{q}_*$ at $t = 0$, as in the case of a breakup, an alternate expression can be given. In this case

$$f(\mathbf{q}, \mathbf{p}, 0) = \delta(\mathbf{q} - \mathbf{q}_*) G(\mathbf{p})$$

according to equation (18), and the collision probability becomes

$$p(\Delta, T) = \frac{1}{N} \int_{\mathcal{O}} G(\mathbf{p})\, d\mathbf{p}\,, \tag{56}$$

where $\mathcal{O} = \{\mathbf{p}: \ |\mathbf{Q}(\mathbf{q}_*, \mathbf{p}, t) - \mathbf{q}_R(t)| < \Delta \text{ for } t \in (0, T)\}$ and $\mathbf{Q}$ is the propagator function (equation (13b)). The subset $\mathcal{O}$ consists of all momenta $\mathbf{p}$ for which the initial condition $(\mathbf{q}_*, \mathbf{p})$ leads to a collision in the interval $(0, T)$.

With regard to numerical calculations, the second formulation, (56), is preferable whenever it is applicable. In either case however the brunt of the calculation is the determination of the domain of integration (either $\mathcal{U}$ or $\mathcal{O}$).

To proceed as far as possible analytically, we shall consider the case of slow dispersion from a reference orbit. The results of the subsection on variational equations are then applicable. From equation (25) we have

$$\mathbf{q} = V\mathbf{p}_0; \tag{57}$$

therefore the inequality

$$|\mathbf{q} - \mathbf{q}_R| < \Delta$$

is equivalent to

$$\mathbf{p}_0 \cdot (V^T V \mathbf{p}_0) - 2\mathbf{p}_0 \cdot (V\mathbf{q}_R) + \mathbf{q}_R^2 < \Delta^2 \tag{58}$$

or

$$\mathbf{u} \cdot (V^T V)\mathbf{u} < \Delta^2 , \tag{59}$$

where

$$\mathbf{u} = \mathbf{p}_0 - V^{-1}\mathbf{q}_R .$$

Since $\det (V^T V) = (\det V^T)(\det V) = (\det V)^2 > 0$, equation (59) places $\mathbf{p}_0$ inside an ellipsoid with center at $V^{-1}\mathbf{q}_R$. The set $\mathcal{O}$ is then the union of all these ellipsoids for $t \in (0, T)$. We have been unable to find an analytic expression for this union, so a numerical procedure has been devised to calculate $p(\Delta, T)$. For the Keplerian case $\sigma = 2$, and for the case of a planar breakup the following numerical procedure was successful. The interval $(0, T)$ was subdivided, and at each division point the inequality (58) was tested at each point of a grid in momentum space using equation (41b). The set is then approximated by those grid points at which the inequality is satisfied. The integral (55) is then calculated numerically based on this grid.

In Fig. 14 we show the results of this calculation for two sets of initial conditions. The ensemble statistics were indentical to the numerical example treated in earlier. This example has the interesting feature that the reference particle which was initially farther away from the breakup point (curve (a)) ultimately acquired the higher probability of collision. The initially closer reference particle (curve (b)) shows a more rapid initial increase in collision probability however. These results illustrate the importance of defining the probability of collision over a time interval rather than instantaneously.

In statistical problems of this sort it is often useful to calculate ensemble averages of quantities. As an example of this, we shall calculate the ensemble average of the square of the distance from the reference particle to members of the continuum. This involves an integration of the product of the left-hand side of (58) and $f(\mathbf{q}, \mathbf{p}, t)$ over all momenta. The result for a two-dimensional Gaussian distribution

$$G(\mathbf{p}) = e^{-(p_1 - b_1)^2/\alpha_1^2 - (p_2 - b_2)^2/\alpha_2^2}$$

is

$$\overline{d^2} = \sum_{i=1}^{2} \left(\frac{1}{2}\beta_i^2 + c_i^2 \right) A_{ii} + 2c_1 c_2 A_{12} ,$$

where

$$c_i = b_i - \mathrm{ent}_i(V^{-1}\mathbf{q}_R)$$

(in which ent means entry) and

$$A_{ij} = \mathrm{ent}_{ij}(V^T V) .$$

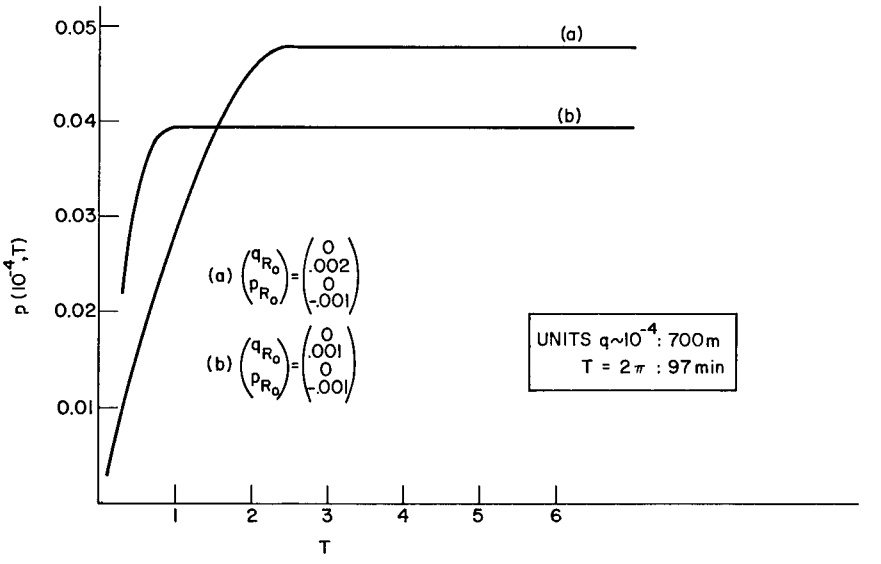

Fig. 14—Probability of collision for two sets of initial conditions

An example of numerical values of $\sqrt{\overline{d^2}}$, a measure of "mean" distance to the continuum particles, is shown in Fig. 15.

To obtain these results it has been assumed that the distribution function for the continuum is known. In reality this will not be the case. To calculate the probability of collision with an actual breakup, one must first solve the inverse problem discussed earlier. Once this has been accomplished, the results of this section may be applied.

CONCLUSIONS

The following concluding remarks are in order:

- The dual time-dependent and time-independent analysis described herein appears to be an effective tool in the determination of the breakup time and place of an orbital explosion from tracking data on the individual fragments.

- Although the time of breakup may be only approximately determined in some cases by the time-dependent procedure, the time-independent analysis can be used to compute the position of the breakup if not the time.

- Breakups with a high-velocity dispersion may be more effectively analyzed than those with low-velocity dispersions.

- Methods of statistical mechanics may be used effectively to study both the evolution of the fragment cloud and the deduction of conditions (time, velocity distribution, etc.) at disintegration. Considerable savings in computer time are possible, because it is not necessary to calculate large numbers of individual trajectories.

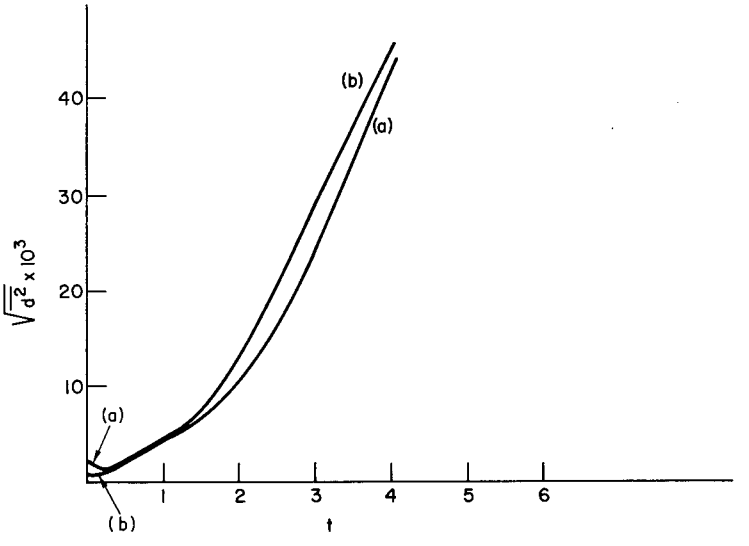

Fig. 15—Ensemble average of mean distance squared

ACKNOWLEDGMENTS

The authors thank Mr. John Gabbard of NORAD for supplying some of the data necessary for our investigation. Also specific appreciation is extended to Messrs. R. Cox, R. Cote, and R. Smith of NAVSPASUR for supplying the data on the Cosmos 699 breakup.

Special thanks go to Mr. J. Alvarez of NASA-Langley for his support and interest in this project.

REFERENCES

1. J.R. Gabbard, "Orbits of Fragments From Exploded Satellites," NORAD/CONAD/ ADC Technical Memorandum 74-3, Nov. 1975.
2. D.R. Brooks, G.G. Gibson, and T.D. Bess, "Predicting the Probability that Earth-Orbiting Spacecraft Will Collide With Man-Made Objects in Space," International Astronautical Federation, 25th Congress, Amsterdam, Sept. 30, 1974.
3. S. Ross, "The Orbital Motion of Pellet Clouds," *J. Astronaut. Sci.* 8(No. 3), 79 (Fall 1961).
4. J.T. Fuss, "Dynamics of Explosion Remnants in Earth-Orbits," Master's Thesis, Old Dominion University, July 1974.
5. J.W. McCarter, "Probability of Satellite Collision," NASA TM X-64671, Washington, D.C., June 8, 1972.
6. R. Cox, R. Cote, and R. Smith, private communication NAVSPASUR, Dahlgren, Va., June 20, 1975.

7. C.G. Hilton and J.R. Kuhlman, "Mathematical Models for the Space Defense Center," Philco Ford Aeronutronic Div., Publication U-3871, Nov. 30, 1966.

8. J.L. Arsenault, L. Chaffee, and J.R. Kuhlman, "General Ephemeris Routine Formulation Document," ESD-TDR-64-522, Aeronutronic Publication U-2731, Aug. 1964.

9. G. Contopoulos, p. 169 in *Space Mathematics*, Part 1, J.B. Rosser, editor, Amer. Math. Soc., 1966.

10. R.G. Langebartel, "Liouville's Equation and the n-Body Problem," Goddard Spaceflight Center Preprint G-575, 1964.

11. W.B. Heard, "Dispersion of Ensembles of Non-interacting Particles," *Astrophys. and Sp. Sci* (in press), 1976.

12. S. Chandrasekhar, *Principles of Stellar Dynamics*, Dover, New York, 1960, p. 83.

13. B. Friedman, *Principles and Techniques of Applied Mathematics*, Wiley, New York, 1956.

14. J.M.A. Danby, "Matrix Methods," p. 32 in *Space Mathematics*, Part 1, J.B. Rosser editor, Amer. Math. Soc., 1966.

15. A. Deprit and A. Deprit-Bartholeme, "The Matrizants of Keplerian Motions (The Two-Dimensional Case)," *Bull. Aston.*, Ser. 3, 3, 315 (1968).

16. W.H. Goodyear, "Completely General Closed-Form Solution for Coordinates and Partial Derivatives for the Two-Body Problem," *Astron J.* **70**, 189 (1965).

17. J.M.A. Danby, "Integration of the Equations of Planetary Motion in Rectangular Coordinates," *Astron. J.* **67**, 287 (1962).

18. W.H. Goodyear, "A General Method of Variation of Parameters for Numerical Integration," *Astron. J.* **70**, 524 (1965).

19. C.L. Siegel, *Vorlesungen über Himmelsmechanik*, Springer Verlag, Berlin, 1956.

20. L.A. Pars, *A Treatise on Analytical Dynamics*, Wiley, New York, 1965.